

TIME-SERIES PHOTOMETRY OF STARS IN AND AROUND THE LAGOON NEBULA. I. ROTATION PERIODS OF 290 LOW-MASS PRE-MAIN-SEQUENCE STARS IN NGC 6530

CALEN B. HENDERSON¹ AND KEIVAN G. STASSUN^{2,3,4}

Draft version May 12, 2019

ABSTRACT

We have conducted a long-term, wide-field, high-cadence photometric monitoring survey of $\sim 50,000$ stars in the Lagoon Nebula H II region. This first paper presents rotation periods for 290 low-mass stars in NGC 6530, the young cluster illuminating the nebula, and for which we assemble a catalog of infrared and spectroscopic disk indicators, estimated masses and ages, and X-ray luminosities. The distribution of rotation periods we measure is broadly uniform for $0.5 < P < 10$ d; the short-period cutoff corresponds to breakup. We observe no obvious bimodality in the period distribution, but we do find that stars with disk signatures rotate more slowly on average. The stars' X-ray luminosities are roughly flat with rotation period, at the saturation level ($\log L_X/L_{\text{bol}} \approx -3.3$). However, we find a significant positive correlation between L_X/L_{bol} and co-rotation radius, suggesting that the observed X-ray luminosities are regulated by centrifugal stripping of the stellar coronae. The period–mass relationship in NGC 6530 is broadly similar to that of the Orion Nebula Cluster (ONC), but the slope of the relationship among the slowest rotators differs from that in the ONC and other young clusters. We show that the slope of the period–mass relationship for the slowest rotators can be used as a proxy for the age of a young cluster, and we argue that NGC 6530 may be slightly younger than the ONC, making it a particularly important touchstone for models of angular momentum evolution in young, low-mass stars.

Subject headings: stars: pre-main-sequence — stars: rotation — NGC 6530

1. INTRODUCTION

Time-domain photometric monitoring surveys of young stars have been crucial to our understanding of a variety of fundamental questions related to low-mass stars in the pre-main-sequence (PMS) phase of evolution. Indeed, our empirical understanding of time-variable accretion processes (e.g. Gullbring & Gahm 1996; Bouvier et al. 1999; Stassun & Wood 1999; Bouvier et al. 2004), of magnetic activity (e.g. Walter et al. 1987; Feigelson et al. 2002, 2005, 2007; Walter et al. 2004; Stassun et al. 2004a, 2006b, 2007b), of the early evolution of stellar angular momentum (e.g. Attridge & Herbst 1992; Bouvier et al. 1993; Choi & Herbst 1996; Stassun et al. 1999; Rebull 2001; Herbst et al. 2002; Makidon et al. 2004; Lamm et al. 2005; Irwin et al. 2008a,b), of the inner architectures of protoplanetary disks (e.g. Bouvier et al. 2003; Winn et al. 2006; Bouvier et al. 2007; Herbst et al. 2008, 2010), of the formation of binary stars (e.g. Mathieu et al. 1997; Basri et al. 1997; Jensen et al. 2007; Stassun et al. 2008), of outbursts (e.g. Walter et al. 2004; Briceño et al. 2004; Kastner et al. 2004; Grosso et al. 2005; Aspin et al. 2006; Aspin 2011; Covey et al. 2011; Bastien et al. 2011), of pulsations (e.g. Zwintz & Weiss 2006; Guenther et al. 2007), and of the fundamental masses and radii of PMS stars (e.g.

Casey et al. 1998; Covino et al. 2000; Stassun et al. 2004b, 2006a, 2007a; Irwin et al. 2007; Stempels et al. 2008; Stassun et al. 2008; Hebb et al. 2010), has relied upon detailed light curves of T Tauri stars (TTs) in a variety of young clusters and star-forming regions spanning a range of ages and star-forming environments.

The most extensively monitored regions include the Taurus-Auriga association (age ~ 1 –3 Myr), the Orion Nebula Cluster (~ 1 –2 Myr), NGC 2264 (~ 3 Myr), NGC 2362 (~ 3 –4 Myr), IC 348 (~ 4 –5 Myr), and NGC 2547 (~ 40 Myr). At a distance of ~ 400 pc (e.g. Menten et al. 2007), the Orion Nebula Cluster (ONC) and the larger star-forming region surrounding it is the nearest and perhaps the single best-studied massive star-forming region. This region contributes photometrically-determined rotation periods for hundreds of TTs (see Herbst et al. 2007, and references therein), nearly all of the known PMS eclipsing binary stars (see Stassun et al. 2009, and references therein), including the only brown-dwarf eclipsing binary system yet discovered (Stassun et al. 2006a, 2007a; Gómez Maqueo Chew et al. 2009; Mohanty et al. 2009, 2010), and the most well-studied FUor/EXor type eruptive star discovered in recent times (V1647 Ori; see, e.g., Bastien et al. 2011, and references therein). Thanks in large part to the broad array of discoveries enabled by the extensive photometric monitoring surveys of this region, the ONC has become a crucial testbed for star formation theory, from PMS angular momentum evolution (see Stassun & Terndrup 2003; Herbst et al. 2007) to the nature of the initial mass function (see Hillenbrand 1997; Da Rio et al. 2010). As wide-area photometric monitoring campaigns begin to survey a larger number of star-forming regions, particularly rich young clusters like

¹Department of Astronomy, The Ohio State University, 140 W. 18th Ave., Columbus, OH 43210, USA; henderson@astronomy.ohio-state.edu

²Department of Physics & Astronomy, Vanderbilt University, VU Station B 1807, Nashville, TN 37235, USA

³Department of Physics, Fisk University, 1000 17th Ave. N., Nashville, TN 37208, USA

⁴Department of Physics, Massachusetts Institute of Technology, 77 Massachusetts Ave., Cambridge, MA 02139, USA

the ONC, the discovery space is becoming enlarged for larger samples of benchmark PMS objects. For example, the recent PTF surveys of the 25 Ori and North America/Pelican nebulae have already resulted in the discovery of numerous new candidate PMS eclipsing binaries and new FUor/EXor outburst systems (van Eyken et al. 2011; Covey et al. 2011).

In this paper we report the first results of a large-scale, multi-year, high-cadence photometric monitoring survey of the bright Lagoon Nebula (Messier 8) H II star-forming region. The massive star cluster illuminating the nebula, NGC 6530, includes a rich population of $\gtrsim 1100$ stellar members spanning the full IMF, from massive OB type stars down to at least the hydrogen burning limit (Damiani et al. 2004; Prisinzano et al. 2005; Damiani et al. 2006; Prisinzano et al. 2007). With a nominal age of ~ 1 Myr (e.g. Mayne et al. 2007), NGC 6530 is thus in many respects an analog of the ONC, but at a distance of ~ 1.25 kpc NGC 6530 provides an ONC-like stellar laboratory beyond the immediate solar neighborhood.

An extensive literature has emerged over the past few years, characterizing the PMS population of NGC 6530 from X-ray to infrared wavelengths. Damiani et al. (2004) conducted the first large-scale study of the stellar population of NGC 6530. Using *Chandra* they detected 884 X-ray point sources, finding that 90–95% of them constitute cluster members. Prisinzano et al. (2005) subsequently performed a complementary deep optical survey of the region, obtaining BVI_C photometry down to $V \approx 23$ using the Wide Field Imager at the MPG/ESO 2.2m telescope. They matched their catalog to that of Damiani et al. (2004) and found 828 common stars, the vast majority of which are cluster members. From their deep color-magnitude diagrams (CMDs) and X-ray membership selection, they determined a cluster distance of 1.25 kpc and a modest cluster extinction of $A_V = 1.1$ mag, and they moreover estimated masses and ages for the stars through comparison with the PMS evolutionary tracks of Siess et al. (2000). Damiani et al. (2006) performed a near-infrared (NIR) survey of the cluster to identify stars with NIR excess emission indicative of objects bearing massive protoplanetary disks, and in the process increased the number of PMS cluster members to more than 1100. Prisinzano et al. (2007) spectroscopically studied a subsample of 332 cluster members, using H α emission to classify the stars as classical T Tauri stars (CTTSs) or weak-lined T Tauri stars (WTTSs).

Our synoptic survey of the photometric variability properties of NGC 6530 builds on these studies. Our light curves of a $40' \times 40'$ region centered on NGC 6530 include the known cluster members as well as a total of $\sim 50,000$ other stars within and surrounding the larger Lagoon Nebula star-forming region. These light curves in concert with the extant literature enable an array of variability studies for the region, including measurement of stellar rotation periods, identification of PMS eclipsing binaries, characterization of accretion induced variations and stellar occultations due to disk obscuration, and discovery of eruptive variables. This first paper presents the results of our systematic search for rotation periods among the members of NGC 6530, the first such survey for stellar rotation periods yet reported for this important cluster.

Understanding the evolution of stellar angular momentum, particularly during the first few Myr of a star’s life, remains one of the longest outstanding questions in star formation research (e.g. Vogel & Kuhi 1981; Hartmann et al. 1986; Bouvier et al. 1986). As PMS stars contract toward the main sequence, they would be expected to rapidly spin up to near breakup velocity as a consequence of angular momentum conservation. However, numerous surveys of rotation periods among low-mass PMS stars clearly show that these stars typically rotate at a small fraction of breakup, despite significant contraction in stellar radius (e.g. Stauffer & Hartmann 1987). A variety of mechanisms for efficiently removing angular momentum from PMS stars during the first ~ 10 Myr has been proposed, including magnetic star-disk interaction (i.e., “disk-locking”; Koenigl 1991; Shu et al. 1994; Najita 1995; Ostriker & Shu 1995), scaled-up solar-type magnetized winds perhaps driven by accretion (e.g. Matt & Pudritz 2004, 2005b,a, 2008a,b), and scaled-up solar-type coronal mass ejections (e.g. Aarnio et al. 2009, 2010, 2011). However, the observational support for and theoretical efficacy of these mechanisms remains debated. There is not yet a consensus on the dominant mechanism(s) responsible for governing the angular momentum evolution of low-mass PMS stars.

In contrast, by the time a young cluster of stars reaches the age of the Pleiades (~ 125 Myr), the observational picture is much more clear. By Pleiades’ age, a cluster of coeval stars develops two distinct populations in period versus mass, now commonly referred to as the “I” and “C” sequences (Barnes 2003, 2007; Barnes & Kim 2010; Barnes 2010). These respectively correspond to curves that trace the upper and lower envelopes of stellar rotation periods. At an age of ~ 600 Myr, about the age of the Hyades, nearly all stars inhabiting the “C” sequence will have spun down and transitioned onto the “I” sequence. This general behavior is attributed principally to changes in the stars’ internal structures as a function of mass, and has been found to hold true for clusters at a variety of ages (Patten & Simon 1996; Barnes et al. 1999; Allain et al. 1996; Krishnamurthi et al. 1998; Radick et al. 1987, 1990). While this “gyrochronology” paradigm has yet to be extended back to the PMS stage, it is clear that young low-mass stars must at some stage prior to the main sequence develop specific relationships between rotation period and stellar mass, and that these encode the stellar age. Exploiting the very young age of NGC 6530, we are in a position to better define the initial conditions of PMS angular momentum evolution, and to identify when and how the period–mass–age relationship begins to take shape.

In this paper we report rotation periods for 290 members of NGC 6530. We match these to the literature to produce a catalog with which we investigate correlations between rotation period and other stellar properties, including disk presence, mass, age, spatial distribution within the cluster, and X-ray activity. In §2 we describe the photometric observations and their reduction, data from the literature, and the construction of our catalog. Our period search and statistical methods are discussed in §3. In §4 we examine the distribution of rotation periods, and investigate correlations between rotation period and the other stellar properties in our

catalog. We discuss the implications of our results in §5, and in §6 we summarize the main conclusions.

2. DATA

2.1. Observations

We have photometrically monitored the Lagoon Nebula over a period of several years using the SMARTS 1.0-meter and 0.9-meter telescopes at the Cerro Tololo Inter-American Observatory (CTIO). Table 1 summarizes the observing runs, the telescope used, and the number of nights with useable data for each. For this paper we use the data from the longest of the observing runs, in June–July 2006.

We repeatedly imaged the Lagoon Nebula on 27 clear nights over a time baseline spanning the 35 nights from June 15 to July 19. We used the Y4Kcam on the SMARTS 1.0-meter telescope at CTIO. The observations consist of 720 s exposures taken through the Cousins *I* filter. The Y4Kcam has a field of view (FOV) of $20' \times 20'$ square, and we imaged four fields, alternating imaging each one. This gives us a full FOV of $40' \times 40'$ square which we imaged with a sampling cadence of $\sim 1 \text{ hr}^{-1}$. The field was centered on the NGC 6530 cluster, $(\alpha, \delta) = (18^{\text{h}}04^{\text{m}}24^{\text{s}}.2, -24^{\circ}21'06''.0)$ (J2000.0), the same as the *Chandra* observation of Damiani et al. (2004).

Table 2 gives an overview of the observations used in this paper. Figure 1 shows a $1 \times 1 \text{ deg}^2$ image of the region with overlays of this study and the X-ray study of Damiani et al. (2004).

2.2. Data Reduction

The images were reduced, and instrumental magnitudes for all point sources extracted, using standard IRAF⁵ procedures. Differential light curves were determined from PSF photometry using an algorithm for inhomogeneous ensemble photometry (Honeycutt 1992) as implemented in Stassun et al. (1999, 2002) for observations of high-nebulosity regions such as M8. We used a point-source detection threshold of 7σ above the sky background noise, and we kept only sources detected in at least 50 frames.

Figure 2 shows the r.m.s. of the light curves as a function of I_C magnitude (calibrated using the absolute photometry of Prisinzano et al. 2005) for each of the 53,500 stars in our images. In the figure, the lower envelope of points with declining r.m.s. toward brighter I_C magnitude represents intrinsically non-variable stars to within the precision of our photometry, which is $\sim 0.008 \text{ mag}$ at $I_C \approx 14$ and rising to $\sim 0.04 \text{ mag}$ at $I_C \approx 18.0$ (the faint limit of our period search; see below). The rising envelope of r.m.s. for bright stars with $I_C \lesssim 14$ is due to CCD non-linearity effects for stars approaching saturation ($I_C \approx 12.5$), and so we limit our period search to stars with $I_C \geq 13.0$ (see below).

We determined astrometric positions for each star in our catalog using the `astrometry.net` tool suite (Lang et al. 2010). The absolute positions of our sample stars are expected to be accurate to $\lesssim 1''$.

⁵ IRAF is distributed by the National Optical Astronomy Observatory, which is operated by the Association of Universities for Research in Astronomy under cooperative agreement with the National Science Foundation.

2.3. Data from the Literature

Large-scale X-ray observations of young clusters have demonstrated that X-ray emission is a highly efficient means for separating low-mass PMS stars from field contaminants (e.g. Getman et al. 2005b,a; Güdel et al. 2007; Feigelson et al. 2011). For example, the *Chandra* Orion Ultradeep Project (COUP) found the rate of contaminants (due to foreground/background field stars and extragalactic sources) to be $< 10\%$ (Getman et al. 2005a). Thus we begin with the X-ray catalog of NGC 6530 from Damiani et al. (2004) to identify the most likely cluster members. They expect contamination in their population from non-member field stars to be $\sim 5\%$.

First we match each of the stars in our photometric database to the Damiani et al. (2004) X-ray source list using a positional tolerance of $2''$. From this we determined the mean offsets between the two astrometric systems for each of our fields, which are listed in Table 3 (where offsets are positionally calculated as Damiani–ours), and corrected our astrometry to place all of the stars onto the Damiani et al. (2004) system. Then we re-matched our stars to the Damiani et al. (2004) catalog employing a $1.5''$ tolerance. This results in 662 unique cluster members which form the master sample for the present study. For these stars we also derive X-ray luminosities from the X-ray count rates reported by Damiani et al. (2004).

Stellar masses and ages come from the optical catalog of Prisinzano et al. (2005), and we use the isochrones of Siess et al. (2000) to infer stellar bolometric luminosities. We identify stars likely possessing warm, massive circumstellar disks using two different indicators—the reddening-free index of NIR-excess, Q_{VIJK} , reported by Damiani et al. (2006), and the CTTS/WTTS classifications of Prisinzano et al. (2007) and Arias et al. (2007) based on their spectroscopic survey of H α emitting stars in the cluster. Finally, known spectroscopic binaries are identified from the catalog of Prisinzano et al. (2007).

Figure 3 shows the V versus $V - I_C$ CMD for our X-ray selected master study sample. The PMS evolutionary tracks of Siess et al. (2000) are overlaid for context (we transformed the tracks from effective temperature and bolometric luminosity to the CMD plane using the main-sequence relations of Kenyon & Hartmann 1995). The sample stars span a range of inferred masses $0.2 \lesssim M/M_{\odot} \lesssim 5$.

3. ANALYSIS

3.1. Period Search

We use the VARTOOLS light curve analysis program (Hartman et al. 2008) to search for periods in our light curves, employing the Lomb-Scargle (LS) period search algorithm (Lomb 1976; Scargle 1982; Press & Rybicki 1989; Press et al. 1992). Because the temporal baseline of our light curves is 35 days, we restrict the search to periods shorter than 20 d, i.e. just over 50% of the baseline. We also limit the search to periods longer than 0.1 d, corresponding to the Nyquist limit given our typical sampling frequency of $\approx 0.05 \text{ d}$ (see §2). We first clipped the light curve data with iterative 3-sigma outlier rejection and then selected only those periods whose peaks in the resulting LS periodogram satisfied a signal-to-noise ratio, $|SNR| > 4.0$.

We perform a Monte Carlo simulation with our observed light curves to determine the false-alarm probability (FAP) of the periods we detect. Following the procedures described in Stassun et al. (1999), for each star we generate 10,000 synthetic light curves from which we empirically determine the distribution of peak heights in the LS power spectrum that would arise from noise. We then compare the height of the peak in the star’s observed LS power spectrum to this distribution of peak heights to determine the FAP. Each of the 10,000 synthetic light curves consists of two sources of noise. The first is the point-to-point scatter in the photometry which we simulate by scrambling the star’s actual light curve data. The second is a correlated noise with a timescale of 1 d, whose amplitude we estimate from the standard deviation of nightly means from the star’s light curve. The former preserves the specific noise distribution and the time sampling pattern of the actual data for each star, while the latter gives the synthetic light curves the freedom to vary on timescales that are long compared to our sampling interval, allowing them to mimic any slow variability of stellar origin (such as accretion activity) that could produce spurious periodic behavior that would be misinterpreted as a rotation period.

We consider “definite” rotation periods to be those with $\text{FAP} \leq 0.001$. In other words, these stars’ LS power spectra evince peaks whose strengths occur by chance in 10 or fewer of the 10,000 noise light curves. As our master sample includes 662 stars, we therefore expect at most ~ 1 false positive period. In addition, we consider “possible” rotation periods to be those with $0.001 < \text{FAP} \leq 0.01$. Throughout our analysis we generally only utilize the definite rotation period stars, but we include the possible rotation period stars here for the benefit of future follow-up studies.

From our master sample of 662 cluster members we find 256 definite periods and 47 possible periods. Finally, for the remainder of our analysis, we include only those stars included in the optical catalog of Prisinzano et al. (2005), for which we have estimated stellar masses and ages. This yields a final catalog of 244 cluster members with definite periods and 46 with possible periods. The sample of 244 definite periods represents the successful detection of periods for one-third of the Damiani et al. (2004) X-ray catalog of NGC 6530 cluster members. The full catalogs of cluster members with definite and possible rotation periods are in Tables 4 and 5, respectively, along with all of the associated data that we have gleaned from the literature (see §2.3). Figure 4 shows the phase-folded light curves of the 244 definite rotators, ordered by increasing period. Figure 5 shows the same for the 46 possible rotators.

The definite and possible rotators are also highlighted in the CMD shown in Figure 3. Our sample of rotators span the range $13.0 \lesssim I_C \lesssim 18.0$. Note that many stars with high r.m.s. are not identified here as rotation period detections because they were not identified as cluster members in the X-ray study of Damiani et al. (2004); future investigations of cluster membership would enable an even larger sample of rotation period determinations for NGC 6530 from our light curves.

We quantify our period detection sensitivity and any biases as functions of period and stellar brightness. We use 1000 of the non-variable stars in our full data set,

and that are in in the same magnitude range as our rotators, as a control sample. For each star we inject sinusoids with amplitude in the range $0.02 \leq \Delta I \leq 0.2$, typical for our sample of rotators (see Fig. 4), into the light curves with periods in the range 0.1–20 d and run the VARTOOLS LS period search algorithm using the same criteria as above. We consider the period successfully recovered if it agrees with the input period to within 10%, which is an acceptable margin of error in the rotation periods for the purposes of our analysis below. Some of the observed light curves for our sample of rotators show modest departures from sinusoidal shapes (see Fig.4), but we expect any resultant errors in the periods to be within the 10% tolerance that we adopt for this test.

Figure 6a shows the fraction of correctly recovered periods as a function of input period, while Figure 6b shows the fraction of correctly recovered periods as a function of I_C magnitude. We find that our period detection efficiency is roughly constant at $\approx 90\%$ for the full range of rotation periods tested. Thus, while this simulation suggests we are missing $\sim 10\%$ of the true underlying population of rotators, with variability amplitudes larger than 0.02 mag, we infer no strong biases in the rotation period distribution as a function of period. At the same time, there is a strong bias against period detection for the bright stars with $I_C \lesssim 14$, clearly the result of the higher r.m.s. in our light curves for the brightest stars (see §2.1). For fainter stars the detection efficiency is approximately 100%, and thus the $\sim 10\%$ loss of efficiency seen in Fig. 6a is entirely a consequence of the brighter stars. However, again, Fig. 6a indicates that this loss of efficiency is largely independent of period, and thus we expect no strong biases in the period distribution of our sample. Figure 6c shows that our detection efficiency is also independent of amplitude over this range. We also performed a simulation with injected amplitudes as low as 0.002 mag and found that our sensitivity remained high down to $\Delta I \sim 0.006$ mag. However, given the simple nature of these simulations (e.g. we inject perfectly sinusoidal signals), we conservatively assume that we are not sensitive to periodic variations below ~ 0.02 mag given the ~ 0.01 mag precision in the photometry.

Finally, we note that 21 of the 244 stars in the definite rotator group have been previously identified as candidate spectroscopic binaries (SB2s; see Table 4). In these cases it is possible that the periodicity we observe is related to the binary orbit but not to the rotation of the star(s), or that the rotation of the star dominating the light has been affected by the presence of a close faint companion star. We do not attempt to correct for these possibilities, but note here that these SB2s constitute less than 10% of our sample and are not concentrated at specific rotation periods, so we do not expect these to alter our results. We do comment on specific interesting cases below. We note that those SB2s with shorter periods could potentially be non-member field contaminants. Our catalog of members with rotation periods is X-ray-selected, and tidally-locked short-period binaries in the foreground might display enhanced X-ray emission that would mimic that of cluster members.

3.2. Correlation Tests

We employ two standard statistical tests to examine possible differences or trends in the rotation periods as a function of various stellar properties: the Kolmogorov-Smirnov (KS) test, which determines the probability that two samples were drawn from the same parent distribution, and the Student’s t test, which determines the probability that two samples possess identical means. For a given stellar property (e.g. mass), we divide the period distribution into two bins (e.g. low-mass and high-mass) and apply these statistical tests on the rotation periods of the two bins. In all of the statistical comparisons below we include only stars with definite rotation periods as defined above (see §3.1).

4. RESULTS

4.1. Period Distribution

Figure 7 shows the rotation period distribution of our entire sample of 244 cluster members with definite periods. The masses and ages for these stars from Prisinzano et al. (2005) using the PMS evolutionary tracks of Siess et al. (2000) are shown in Figure 8. The typical star in our sample is inferred to have M_* $\sim 0.6 M_\odot$ and age ~ 2 Myr according to these tracks (but see §5 for a detailed discussion of the likely age of the cluster). Correlations between the rotation periods and these masses and ages are discussed below.

The distribution is roughly flat for $P \leq 10$ d. A peak is apparent near $P = 1$ d, which may suggest that some aliasing effects at the diurnal sampling frequency of the light curves is still present. Despite this, a one-sided KS test comparing the observed distribution with a uniform distribution for $P \leq 10$ d yields a probability of 18% that the two distributions represent the same parent population. Thus, the null hypothesis—a uniform distribution in this case—is not rejected by the observed period distribution.

We observe two clear cutoffs in the period distribution, despite our good sensitivity to periodic signals for periods both longer and shorter than the observed cutoffs. At the long period end, the distribution tapers off strongly for $P \gtrsim 10$ d. This is very similar to the observed long-period cutoff in the distributions of other young clusters, such as the ONC (e.g. Stassun et al. 1999). At the short-period end, the distribution drops dramatically for $P \lesssim 0.5$ d. For the typical star in our sample, with $M_* \approx 0.6 M_\odot$ and $R_* \approx 2.2 R_\odot$ (according to the PMS tracks of Siess et al. 2000), the rotation period corresponding to breakup velocity is ≈ 0.5 d. Therefore, we ascribe the short-period cutoff to a real physical limit on the minimum rotation period for the stars in our sample.

4.2. Disk and Accretion Indicators

We use the reddening-free index of NIR excess, Q_{VIJK} (Damiani et al. 2006), to segregate our sample according to the likelihood that they possess massive circumstellar disks. Those stars that are identified in Damiani et al. (2006) as having a high Q_{VIJK} value display significant IR emission relative to their optical color, and we adopt their same classifications to indicate which stars harbor a circumstellar disk. We note that Q_{VIJK} is a fairly crude measure of NIR excess, and certainly does not yield information on disk structure. Stars without large Q_{VIJK} index values may still possess disks, for example, if the disk

has an evacuated inner hole. We perform a two-sided KS test as well as a t test to compare the period distributions of the “disked” and “non-disked” stars. Table 6 gives the number of stars in each group and the details of the statistical results. We find that the period distribution for stars with NIR excess is statistically different from those without NIR excess, with a $\sim 1\%$ probability that they were drawn from the same distribution. We also find that the means of the distributions (6.3 d and 3.7 d for the disked and non-disked stars, respectively) have only a $\sim 0.1\%$ probability of being the same (i.e. the difference in means is statistically significant). Figure 9a offers a visual comparison of this result. While those stars with no NIR excess are concentrated at faster periods, those with NIR excess are more uniformly distributed and exhibit a significant long-period component.

We also segregate the sample into accretors and non-accretors based on their classification as a CTTS or WTTS, as determined from their $H\alpha$ emission strength. The distributions are shown in Figure 9b. The number of classified CTTS and WTTS stars is small, however the WTTSs appear to be concentrated at faster rotation periods while the distribution for CTTSs is shifted toward longer periods. To quantify the comparison we again perform a two-sided KS tests as well as a t test. The sample sizes and statistical results are in Table 6. The probability that the two period distributions were drawn from the same parent distribution is only $\sim 2\%$, and the probability that their means (7.3 d and 3.4 d for the CTTS and WTTS samples, respectively) are identical is only 0.6%.

4.3. Stellar Mass

Figure 10 shows rotation period as a function of stellar mass (inferred from the PMS evolutionary tracks of Siess et al. 2000) for the sample of NGC 6530 rotators. There is an apparent trend of decreasing rotation period (faster rotation) toward the higher stellar masses. We also show in the figure the stars for which we have NIR excess information (left panel) and the stars for which we have CTTS/WTTS status information (right panel). There is a clear bias present such that almost none of the stars with either NIR excess information or CTTS/WTTS status are present for $M_* < 0.5 M_\odot$. This is the result of the observational limits of the NIR and spectroscopic surveys of the cluster, which were not sensitive to the fainter, low-mass members of the cluster (Prisinzano et al. 2007; Arias et al. 2007).

As an initial quantitative measure of the dependence of rotation period on stellar mass, we divide the sample of rotators into two groups of comparable size based on the overall distribution of the stellar masses (see Fig. 8): a “low mass” group with $M_* \leq 0.5 M_\odot$, and a “high mass” group with $M_* > 0.5 M_\odot$. We chose the mass cut to be at $0.5 M_\odot$ because previous studies have suggested a change in the behavior of the period distribution at around $0.4 M_\odot$ (for the Siess et al. (2000) tracks used here), but dividing the sample at $0.4 M_\odot$ would have created imbalanced groups (63 “low-mass” stars to 181 “high-mass” stars) for definite rotators in our catalog. We have checked that all statistical results reported below based on this mass division are not changed qualitatively if we instead cut on $0.4 M_\odot$. Figure 11 compares the period distributions of these two mass group-

ings, which are clearly different. A KS test gives that the probability of the two period distributions being drawn from the same parent distribution is only 0.1%, and a t test gives a probability of only 0.5% that the means of the two period distributions are identical (see Table 6). The high-mass stars rotate faster than the low-mass stars; their mean rotation periods are 4.9 d and 6.4 d, respectively (Table 6).

4.4. Stellar Age

Figure 12 shows rotation period as a function of age (inferred from the isochrones of Siess et al. 2000) for our sample of NGC 6530 rotators. Here any trends between the rotation periods of the stars and their inferred ages are more subtle than is the case with stellar mass (see above). The stars with available NIR excess and CTTS/WTTS status indicators are not strongly biased with respect to inferred stellar age.

To quantify any relationship between rotation period and inferred stellar age, we divide the sample into two age groups. Based on the distribution of inferred stellar ages (see Fig. 8b), we divide the stars into a “young” group with $\log(\text{age}/\text{yr}) \leq 6.25$ and an “old” group with $\log(\text{age}/\text{yr}) > 6.25$. As was suggested visually in Fig. 12, a t test does not indicate strong evidence for a statistically significant difference in the mean periods of the two groups (Table 6). However, a KS test does indicate that the young and old stars have only a 1.4% chance of being drawn from the same parent rotation period distribution. We conclude that there is weak evidence for a difference in the rotation period distributions of the stars as a function of inferred stellar age, with the older stars rotating slightly more slowly on average (mean rotation periods 5.9 d and 4.9 d, respectively; Table 6).

4.5. Spatial Distribution

Previous works have suggested evidence for sequential star formation in NGC 6530 and the larger Lagoon Nebula region. For example, Lada et al. (1976) suggested that star formation has progressed from NGC 6530 to Herschel 36, nearby and to the west. Similarly, the X-ray study of Damiani et al. (2004) found evidence for an age gradient in NGC 6530, wherein the younger stars are more concentrated in the southeast and older stars in the northwest (cf. Fig. 12 in that paper).

Figure 13 shows the spatial distribution of our sample of rotators in NGC 6530. Following Damiani et al. (2004) we divide the cluster into quadrants (northwest, southeast, etc.) and perform our statistical tests on the rotation period distributions of the stars in different pairs of quadrants. As shown in Table 6, the Student’s t test does not indicate any statistically significant difference in the mean rotation periods as a function of spatial position. However a KS test does show a modestly significant difference in the period distributions when the southeast quadrant is compared to the northwest quadrant, with a probability of $\sim 1\%$ that the rotation period distributions of the two groups were drawn from the same parent distribution. The mean rotation periods in the southeast and northwest quadrants are 6.2 d and 5.2 d, respectively (Table 6). Together with the age gradient found above, this difference in periods would imply that the younger stars (to the southeast) rotate more slowly on average than the older stars (to the northwest).

However, this is in the opposite sense of the (weak) period-age trend found above, in which the isochronally younger stars rotate more rapidly on average. Thus we conclude that any trends in rotation with isochronal age or with age inferred from spatial location are weak at best and inconsistent in sense.

4.6. X-ray Activity

To investigate the relationship between the rotation period of NGC 6530 cluster members and their X-ray activity, we require estimates of the X-ray luminosities (L_X) and the bolometric luminosities (L_{bol}) of the stars in our sample. Neither of these quantities was tabulated by the previous studies of the cluster, so here we adopt a procedure to provide estimates of both quantities.

To estimate L_X for each star, we use the PIMMS software⁶ we convert the X-ray count rates of Damiani et al. (2004) into X-ray fluxes, using the PIMMS MEKAL model. The model requires as input the temperature of the emitting coronal gas (kT) and the hydrogen column density toward the source. For kT , we adopt the median of the kT distribution found by COUP (Getman et al. 2005b). We adopt an extinction of $A_V=1.1$ to the cluster (Prisinzano et al. 2005), which yields a hydrogen column density of $N_H = 2.431 \times 10^{21} \text{ cm}^{-2}$ (Güver & Özel 2009). Finally, adopting a cluster distance of 1.25 kpc (Prisinzano et al. 2005), we convert the PIMMS X-ray fluxes into L_X . This approach obviously does not take into account potential differences in kT or A_V to individual stars, however as only the X-ray count rates are available from Damiani et al. (2004), a more sophisticated approach is not warranted.

To estimate L_{bol} , we interpolate on the PMS evolutionary tracks of Siess et al. (2000) to obtain the predicted L_{bol} for each star, given the mass and age estimates from Prisinzano et al. (2005) using these same evolutionary tracks.

Figure 14 shows the resulting L_X/L_{bol} of the NGC 6530 rotators as a function of rotation period. As a whole the sample shows a roughly constant L_X/L_{bol} at approximately the “saturation” value of $\log L_X/L_{\text{bol}} \approx -3.3$ (e.g. Pizzolato et al. 2003). However, the most rapidly rotating stars appear to exhibit a systematically reduced L_X/L_{bol} . To quantify this, we perform both a KS test and a Student’s t test comparing the L_X/L_{bol} for rapid rotators with $P < 2.5$ d versus more slowly rotating stars with $P > 2.5$ d (see Table 7). We find a statistically significant difference from both tests, with the mean $\log L_X/L_{\text{bol}}$ for the rapid rotators (-3.56) being lower than that for the slower rotators (-3.37) with a statistical significance of 99.97%.

In addition, we have checked whether our sample of rotators is representative of the underlying population of NGC 6530 members in L_X/L_{bol} . Figure 15 compares the distribution of L_X/L_{bol} for stars with and without a measured rotation period. We again find a very statistically significant difference in the two distributions from both a KS test and a t test. The mean $\log L_X/L_{\text{bol}}$ for the sample of rotators (-3.43) is significantly higher than that for the sample without detected rotation peri-

⁶ Distributed by NASA’s High Energy Astrophysics Science Research Center; <http://heasarc.gsfc.nasa.gov/docs/software/tools/pimms.html>

ods (-3.63). The probability that there is no difference in the mean $\log L_X/L_{\text{bol}}$ of the two samples is 6×10^{-6} (see Table 7).

5. DISCUSSION

Ever since the pioneering efforts of Bouvier and collaborators to measure rotation periods of Tau-Aur stars (e.g. Bouvier et al. 1986, 1993, 1997), and of Herbst and collaborators to measure rotation periods of ONC stars (e.g. Attridge & Herbst 1992; Herbst et al. 1994; Choi & Herbst 1996), a fundamental goal has been to characterize the morphology of the rotation period distribution for young low-mass stars. Early works on the ONC emphasized the apparent bimodality of the period distribution, with peaks around ~ 2 d and ~ 8 d and a deep gap in the distribution around ~ 4 – 5 d (e.g. Attridge & Herbst 1992). In contrast, Stassun et al. (1999) found a unimodal distribution in the ONC. These differing results were subsequently argued to be a manifestation of the mass dependence of the period distribution (e.g. Herbst et al. 2001): a bimodal period distribution for solar-mass stars, a unimodal distribution for lower mass stars, and with the lower mass stars rotating faster than the higher mass stars. Several studies have confirmed these trends in the ONC and in other, slightly older clusters, including NGC 2264, NGC 2362, and IC 348 (e.g. Kearns et al. 1997; Kearns & Herbst 1998; Herbst et al. 2000; Lamm et al. 2005; Cieza & Baliber 2006; Irwin et al. 2008a). Thus a picture has emerged in which young stars at $\gtrsim 1$ Myr exhibit a mass-dependent period distribution that is bimodal at higher masses, in which lower mass stars rotate faster on average, and in which older stars tend to spin faster, presumably due to spin-up as the stars contract toward the main sequence.

The distribution of rotation periods we have measured for NGC 6530 is consistent with a uniform distribution for $0.5 < P < 10$ d; we do not observe obvious bimodality in the period distribution. When we subdivide the sample stars into groups by mass, we do not observe bimodality among the higher mass stars (nor for the lower mass stars), and moreover the lower mass stars rotate more slowly on average. These features of the NGC 6530 period distribution and its dependence on stellar mass differ strongly from the trends discussed above for numerous other clusters with ages $\gtrsim 1$ Myr.

We find that NGC 6530 stars with older isochrone ages rotate more slowly on average than their younger counterparts. The statistical significance of this trend is not strong, but as with the other rotational properties of NGC 6530 noted above, such a trend is in contrast with that expected from the longer-term evolution observed between other extensively-studied young clusters, which show a tendency for stars to spin up modestly between the age of the ONC and that of the Pleiades.

These differences in rotational characteristics between NGC 6530 and the other young clusters might be understood if NGC 6530 represents a population of PMS stars that is significantly younger than the other clusters, such that in particular the higher mass stars in the cluster are having their period distribution shaped from a unimodal one into a bimodal one, and the lowest mass stars in the cluster are actively spinning up so that they will end up spinning faster than their higher mass counterparts. That is, the NGC 6530 stars are

perhaps currently evolving toward an evolutionary state when their rotational properties would presumably resemble those of the ONC. Indeed, the age of NGC 6530 has been estimated by Mayne et al. (2007) to be similar to, and possibly slightly younger than, the ONC.

In an attempt to more firmly place NGC 6530 in an evolutionary context relative to other well studied young clusters, and motivated by the findings of Irwin et al. (2008a) who suggested patterns with age in the mass–period relationship of young clusters, we show in Figure 16 the rotation periods as a function of stellar mass for NGC 6530 and five other young clusters with extant rotation period measurements. NGC 6530 is shown first, and the other clusters ordered chronologically with ages from Mayne et al. (2007) and Mayne & Naylor (2008). Finally, we also include the zero-age main sequence cluster NGC 2516. The six clusters from ONC to NGC 2516 thus span a range of ages from ~ 2 Myr to ~ 150 Myr. The period–mass relationship for NGC 6530 as expected appears most similar to that seen in the ONC. Broadly speaking, whereas the older clusters exhibit an increasing tendency for the upper envelope of rotation periods to slope downward at low stellar masses, the upper envelope of rotation periods in NGC 6530 is, like the ONC’s, roughly flat with stellar mass. However, whereas the ONC does exhibit a modest downward slope toward decreasing stellar masses (i.e. the lowest mass stars in the ONC rotate on average faster than the higher mass stars), in NGC 6530 the trend is in the opposite sense (i.e. the lowest mass stars rotate on average more slowly; see §4.3), and this appears in Fig. 16 as a slightly upward slope in the upper envelope of NGC 6530 rotation periods.

To better quantify these trends of rotation period with mass, we fit a linear trend line to the upper envelopes of the rotation periods versus mass for each of the clusters in Fig. 16 (shown as red lines) as follows. For stars with masses in the range $0.5 < M/M_\odot < 0.1$, we grouped the stars into mass bins $0.1 M_\odot$ wide, and within each of these mass bins we calculated the rotation period corresponding to the 75%-ile of the rotation periods in that bin. (We chose the 75%-ile because it is a more robust measure of the upper envelope of the distribution than, e.g., taking the upper-most data point in the bin.) We calculated the uncertainty on the 75%-ile periods as the difference between the 75%-ile and the 50%-ile (the median) divided by the square-root of the number of data points in the bin. Finally, we fit a linear least-squares relationship to the binned points of the form $\log P = a \times M + b$, where a and b are free parameters of the fit. The resulting slopes a and their formal uncertainties are shown plotted versus the age of each cluster in Figure 17, in which we see a clear relationship of increasing slope with increasing age for the younger clusters with ages $\lesssim 10$ Myr and a flattening of the relationship for the two oldest clusters at $\gtrsim 40$ Myr. For specificity, the ages we assigned to each cluster are from Mayne & Naylor (2008, cf. their Table 9), except that for NGC 2362 we adopted an age of 3.5 Myr because its age was estimated as 3 Myr (Mayne & Naylor 2008) and 4 Myr (Mayne et al. 2007), and for IC348 we adopted 4.5 Myr as its age was estimated by Mayne & Naylor (2008) as 4–5 Myr. These cluster ages are summarized in Table 8.

For our linear fit in Fig. 17 (solid line) we did not include NGC 6530; rather, we placed the point corresponding to NGC 6530 at the age at which the 1-sigma upper limit for its rotation period versus mass slope exactly lies on the linear trend fitted to the other clusters. The maximum age inferred for NGC 6530 by this procedure is 1.65 Myr, as compared to the 2 Myr age assigned to the ONC. In addition, the fit to the younger clusters was extended to only 6 Myr, as the measurements for the two oldest clusters (NGC 2547 and NGC 2516) clearly indicate that the trend of increasing slope in the period-mass plane with age must flatten at approximately this age (represented by the dotted line in Fig. 17). The linear relationship fitted to the younger clusters (solid line in Fig. 17) has the form

$$a = 5.98(\pm 1.11) \times \tau - 1.50(\pm 0.61), \quad (1)$$

where a is the slope of the linear relationship between $\log P$ (in days) and M (in M_\odot) for the upper 75%-ile of rotation periods in each cluster over the mass range $0.1\text{--}0.5 M_\odot$, and τ is the cluster age (in Myr). This relationship may be useful for assigning relative ages to PMS stars on the basis of the observed slope in the period-mass relationship.

If NGC 6530 is indeed younger than the ONC, then this implies that the distance to the cluster of 1.25 kpc determined by Prisinzano et al. (2005) must be slightly underestimated. The median age of the stars in our sample inferred from the PMS isochrones of Siess et al. (2000) is ~ 2 Myr (see Figs. 3 and 8b), the same as the ONC using these isochrones. However, if the distance to NGC 6530 is taken to be just 15% larger, the median age of the NGC 6530 sample comes in line with our estimate of ~ 1.5 Myr above. Prisinzano et al. (2005) do not quote an uncertainty on their distance determination, but most other recent distance estimates for the cluster are $\sim 25\%$ larger than 1.25 kpc (e.g. van den Ancker et al. 1997; Loktin et al. 1997; Sung et al. 2000), so a 15% revision would not appear to be unreasonable. Indeed, the original X-ray study of Damiani et al. (2004) adopted a distance of 1.8 kpc, and consequently determined a median age for the cluster of just 0.8 Myr from the same PMS isochrones used here (Siess et al. 2000).

The NGC 6530 rotation period distribution shows a strong cutoff for fast rotation periods, $P < 0.5$ d, and we have found that this short-period cutoff corresponds to breakup speed for these stars. A similar short-period cutoff associated with rotation at breakup was observed in the ONC (Stassun et al. 1999). A few stars in our sample are found with $P < 0.5$ d. While rotation at breakup is a possibility for these stars, we note that their light curves are strikingly similar to those of contact binaries. Some of these stars do have prior spectroscopic data in the literature that did not clearly identify them as spectroscopic binaries (see Table 4). However, we note that the spectra of contact binaries can appear highly broadened, and the line splitting might not be readily recognized as such. The discovery of PMS contact binaries would be very significant in the context of binary formation and evolution, and we suggest that these stars be monitored further for indications of radial velocity variations. A few PMS contact binary candidates have also been identified in Orion (Stassun et al. 1999; Rebull 2001; van Eyken et al. 2011).

The X-ray luminosities of the NGC 6530 stars are flat with rotation period, at the saturation level ($\log L_X/L_{\text{bol}} \approx -3.3$; Pizzolato et al. 2003), however the most rapidly rotating stars show significantly lower $\log L_X/L_{\text{bol}}$ suggestive of so-called “super-saturation” (e.g. James et al. 2000). A similar result was found in the ONC by Stassun et al. (2004a). In a recent meta-analysis of rotation and X-ray activity in low-mass stars at a variety of ages, Wright et al. (2011) argued that super-saturation may be the result of the X-ray coronae in very rapidly rotating stars extending beyond the Keplerian co-rotation radius, and consequently the coronae are centrifugally stripped. To examine this idea in the context of our NGC 6530 sample, in Figure 18 we plot $\log L_X/L_{\text{bol}}$ versus the Keplerian co-rotation radius (R_{co}) for our sample, where R_{co} is determined for each star from the measured rotation period and from the mass and radius inferred from the Siess et al. (2000) evolutionary tracks. We find strong evidence for a correlation between these quantities, (shown as the line in Fig. 18), similar to that suggested by Wright et al. (2011). A non-parametric Kendall’s τ rank correlation test yields a positive correlation coefficient of 0.21, and the probability that the two quantities are not correlated is $< 10^{-6}$. The fastest rotators in our NGC 6530 sample—and those with the lowest L_X/L_{bol} on average—have R_{co} in the range of $1\text{--}3 R_*$, whereas the slower rotators in our sample have R_{co} up to $\sim 15 R_*$. The COUP survey (Getman et al. 2005b) found that the coronae of low-mass PMS stars in that study, as inferred from the lengths of the magnetic loops driving the observed powerful X-ray flares, can have extents of up to $\sim 10 R_*$ (Favata et al. 2005; Aarnio et al. 2010). Such coronal radii can be accommodated within R_{co} for the slower rotators in our NGC 6530 sample, but for the faster rotators would extend beyond R_{co} and would thus be unlikely to remain stable against centrifugal forces. Thus, it appears plausible that the correlation we observe between L_X/L_{bol} and R_{co} is the result of the outer coronae of the rapidly rotating stars being increasingly centrifugally stripped, as suggested by Wright et al. (2011).

Stassun et al. (2004a) also found in the ONC that stars with measured rotation periods exhibit significantly higher L_X/L_{bol} on average than ONC stars without rotation periods, and suggested that this might indicate a population of stars rotating more slowly than the observed long-period cutoff in the ONC ($P \gtrsim 10$ d). Our NGC 6530 sample exhibits very similar properties. In particular, we observe a long-period cutoff for $P \gtrsim 10$ d, and moreover we find that NGC 6530 stars that do not exhibit a rotation period signal in our data are less X-ray luminous on average. Perhaps there is a population of more slowly rotating stars in NGC 6530 than our rotation period measurements can reveal. These low L_X stars could still have periodic signals below 0.02 mag amplitudes that we would not detect given the precision of our data (see §3.1). Sensitive $v \sin i$ measurements in NGC 6530 and the ONC are needed to explore this possibility further.

We find evidence that stars in our NGC 6530 sample with NIR excess emission and/or strong H α emission rotate more slowly on average. In other young clusters, an association between NIR excess and slow rotation has been taken as evidence of the braking of stellar rota-

tion through a magnetic star-disk interaction (so-called “disk-locking”). However, it is not clear that disk-locking models actually predict such a correlation of increased NIR excess for slow rotators. A central prediction of most disk-locking models is that the location of the inner truncation radius of the circumstellar disk relative to the co-rotation radius determines the magnitude and sign of the torque experienced by the star. Thus for slow rotators, whose co-rotation radii are large and for which a braking torque would therefore require an even larger inner truncation radius, one might predict less NIR emission for the slow rotators due to the large inner hole in the disk (e.g. Stassun et al. 2001).

Le Blanc et al. (2011) performed detailed modeling of the spectral energy distributions of stars in IC 348 with measured rotation periods in order to assess in detail for each star the location of the inner disk edge relative to co-rotation. Those authors found that the slow rotators in IC 348 tended to possess disks with inner truncation radii at or beyond co-rotation, whereas the rapidly rotating stars tended to possess disks with inner truncation radii within co-rotation, implying that if star-disk interaction is important for the stars then it must be operating with a tendency to torque down the slow rotators and torque up the rapid rotators. In other words, if disks are important for angular momentum evolution in that cluster, then they must be important for stars at all rotation periods, spinning down some stars while spinning up others. Thus, inferring the nature of any star-disk interaction among our sample of rotators in NGC 6530 awaits detailed modeling of the spectral energy distributions of the stars in order to establish whether and how disks may be sculpting the NGC 6530 rotation period distribution.

6. SUMMARY AND CONCLUSIONS

We have photometrically monitored $\sim 50,000$ stars in a $40' \times 40'$ field centered on NGC 6530, the young massive star-forming cluster illuminating the Lagoon Nebula, over 35 nights in the I_C -band with a cadence of 1 hr^{-1} . These observations are intended to complement recent optical, X-ray, and NIR surveys of the region (Damiani et al. 2004; Prisinzano et al. 2005; Damiani et al. 2006; Prisinzano et al. 2007), permitting a comprehensive characterization of the young stellar population in NGC 6530.

From an analysis of periodic variations in our light curves, we measured rotation periods for 290 X-ray selected cluster members of NGC 6530, with masses in the range $0.2 < M/M_\odot < 2.0$. From the findings of Damiani et al. (2004), we expect $\sim 5\%$ of our catalog to be contaminated by non-members, or only ~ 15 stars in our full photometric catalog. We investigated correlations between rotation period and other stellar properties, including mass, age, spatial distribution within the cluster, the presence of circumstellar disks, and X-ray activity. The major findings of this work are as follows:

1. The distribution of rotation periods in NGC 6530 is approximately uniform over the range $0.5 < P < 10 \text{ d}$; we do not observe obvious bimodality in the period distribution, regardless of whether the distribution is considered in its entirety or limited to narrower ranges of stellar mass. The sharp cutoff

in the period distribution at $P \approx 0.5 \text{ d}$ likely results from the breakup limit for the stars in our sample. A small number of stars with $P < 0.5 \text{ d}$ are present, which should be investigated further as possible pre-main-sequence contact binary systems.

2. The X-ray luminosities of the stars are roughly flat with rotation period, at approximately the saturation level ($\log L_X/L_{\text{bol}} \approx -3.3$). However, the fastest rotators show lower average X-ray luminosities, at a highly statistically significant level, suggestive of so-called “super saturation.” At the same time, X-ray luminosity correlates most strongly with the stars’ co-rotation radii, suggesting that centrifugal stripping of the coronae may be the fundamental driver of the super saturation phenomenon.
3. Stars with NIR excesses and $H\alpha$ emission indicative of warm circumstellar material rotate more slowly on average than stars lacking disk signatures. Disked stars might be presumed to be younger on average, and indeed we find evidence that stars with younger ages as inferred from spatial location within the cluster rotate more slowly on average. However, the statistical significance is low, and indeed we find the opposite association between rotation and age when the ages are inferred from PMS isochrones.
4. The rotation periods are a function of stellar mass: the lower mass stars rotate more slowly on average than the higher mass stars. This is in the opposite sense of the period-mass relationship observed in the ONC and in all other slightly older clusters.
5. We show that the slope of the mass-period relationship among slow rotators (defined as the 75%-ile rotation periods) in the mass range $0.1 < M/M_\odot < 0.5$ is a good proxy for the age of a young cluster. Calibrating this empirical mass-period-age relation to the ONC, NGC 2264, NGC 2362, IC348, NGC 2547, and NGC 2516, we find that NGC 6530 is the youngest of all, with a maximum age of 1.65 Myr on an age scale where the ONC is 2 Myr.

The evidence points strongly to NGC 6530 being in a very early stage of rotational evolution in which the stars are currently evolving toward a state that will presumably resemble the ONC within the next $\lesssim 1 \text{ Myr}$. Thus NGC 6530 becomes an important new touchstone for theoretical models of angular momentum evolution in young, low-mass stars.

An important question that remains to be resolved is the role of circumstellar disks in the rotational evolution of these stars. The observed correlation between NIR excess and slow rotation has been taken in previous studies as evidence for rotational braking via star-disk interaction. However, it is not clear that theories of star-disk interaction in fact predict this correlation. Additionally, recent detailed modeling of the full spectral energy distributions of young stars with rotation periods in IC348 indicate that, if disks do affect the spin rates of the stars, they must act both to spin down some stars and to spin

up others (Le Blanc et al. 2011). A similarly detailed assessment of the disk torques likely being experienced by the stars in NGC 6530 will be important to determine whether and how disks may yet be acting to shape the mass-period relationship in this very young cluster.

Finally, it remains an important challenge to empirically connect the rotational properties of PMS stars to those of main-sequence stars, and to theoretically connect the dominant mechanisms thought to govern the evolution of angular momentum in the PMS to those on the main sequence. Main sequence angular momentum evolution is principally understood through intrinsic structural changes in the stars that, through stellar winds, lead to distinct period-mass relationships that evolve predictably with time and thus permit reliable age-dating of stars (gyrochronology). In contrast, in the PMS phase the dominant angular momentum evolution mechanisms have generally been thought to be extrinsic to the stars (e.g., disk-locking). Yet it is now clear that low-mass stars already evince clear period-mass relationships in the PMS stage. Evidently, as early as the very young age of NGC 6530, a period-mass relationship that can be projected forward to the main sequence is already taking form, and this relationship already encodes stellar age.

We thank Robert Siverd for technical assistance and Soeren Meibom for enlightening discussions. CBH acknowledges the support of the NSF Graduate Research Fellowship #2011082275 and also the NSF-funded Research Experiences for Undergraduates program in Physics & Astronomy at Vanderbilt University. KGS acknowledges support through NSF grant AST-0808072, as well as the generous support and hospitality of a Martin Luther King Visiting Professorship at the Massachusetts Institute of Technology.

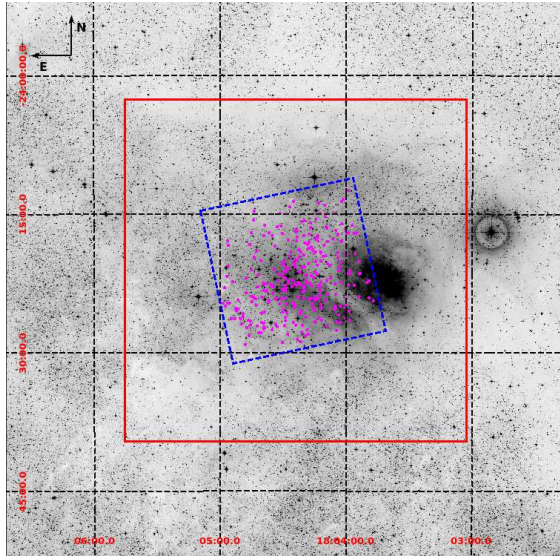


FIG. 1.— A NASA SkyView image of the region around NGC 6530. The image size is $1 \times 1 \text{ deg}^2$ and centered on $(\alpha, \delta) = (18^{\text{h}}04^{\text{m}}24^{\text{s}}.4, -24^{\circ}21'06''.0)$ with north up and east to the left. The area covered by this study is shown in red while the X-ray study of Damiani et al. (2004) is shown in dashed blue. Our 290 stars with rotation periods are shown in magenta. See the electronic journal for a color version of this figure.

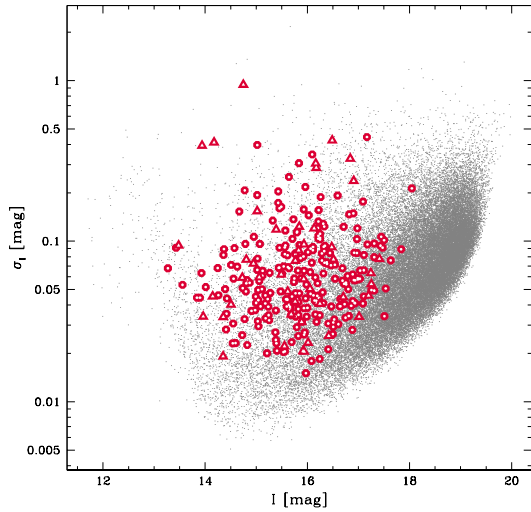


FIG. 2.— RMS of the light curves as a function of calibrated I_C magnitude for the 53,500 stars in our four fields. The red circles denote the 244 stars with “definite” rotation periods ($\text{FAP} \leq 0.001$) while the red triangles mark the 46 stars with “possible” rotation periods ($0.001 < \text{FAP} \leq 0.01$). See the electronic journal for a color version of this figure.

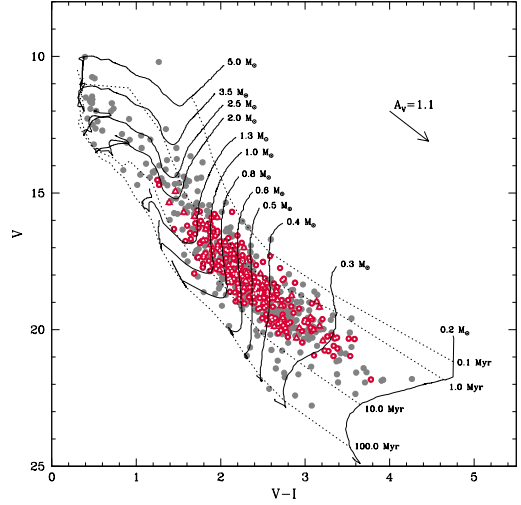


FIG. 3.— V versus $V-I_C$ color-magnitude diagram for our master sample drawn from the catalog of X-ray members of Damiani et al. (2004) (filled symbols). Stars for which we report rotation periods are highlighted. Overplotted are the PMS evolutionary tracks of Siess et al. (2000) assuming a distance of 1.25 kpc and an extinction of $A_V = 1.1 \text{ mag}$ (Prisinzano et al. 2005). The reddening vector shown uses the above A_V and the color excess $E(V-I) = 0.46$ value from Prisinzano et al. (2005). See the electronic journal for a color version of this figure.

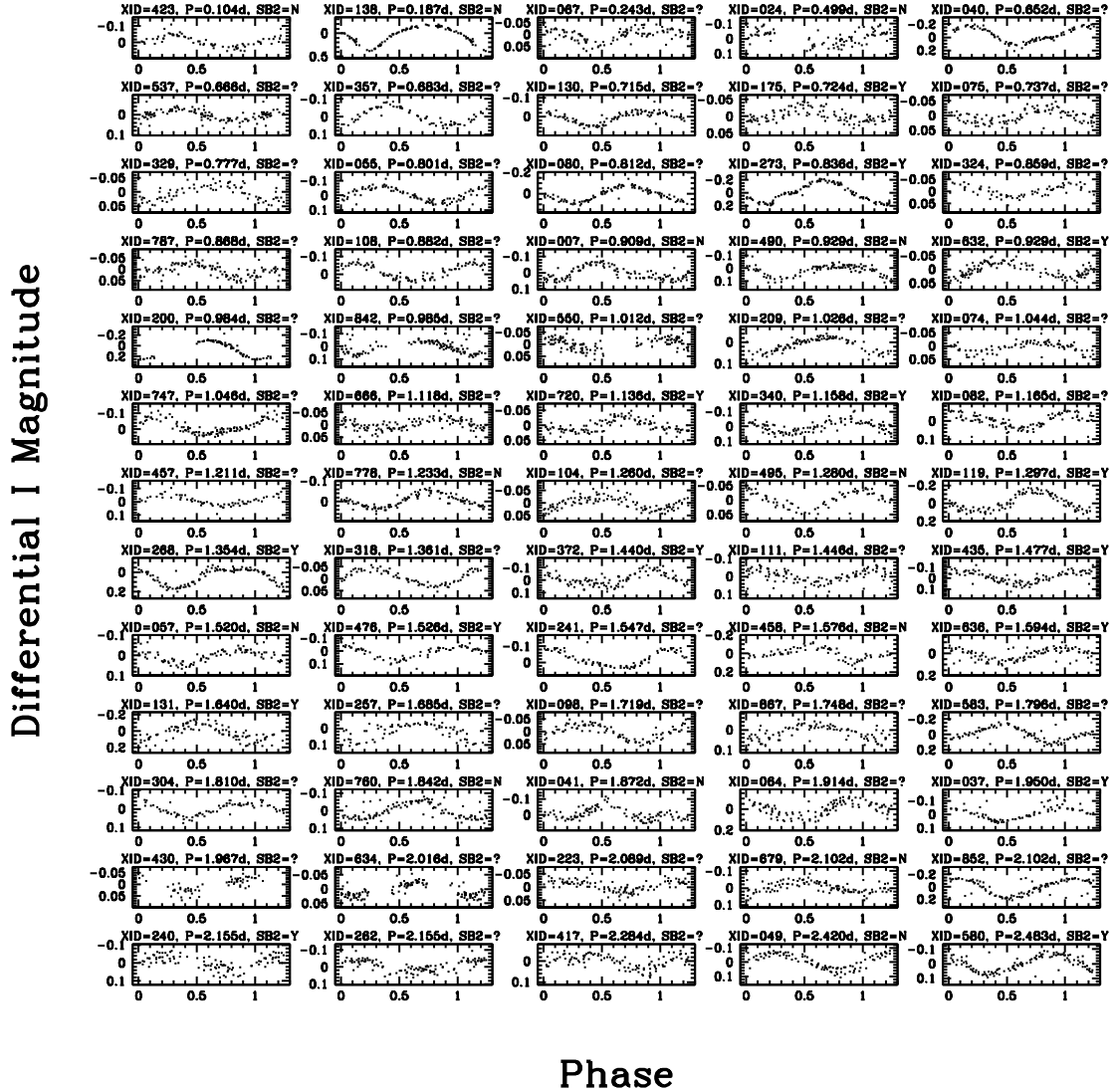
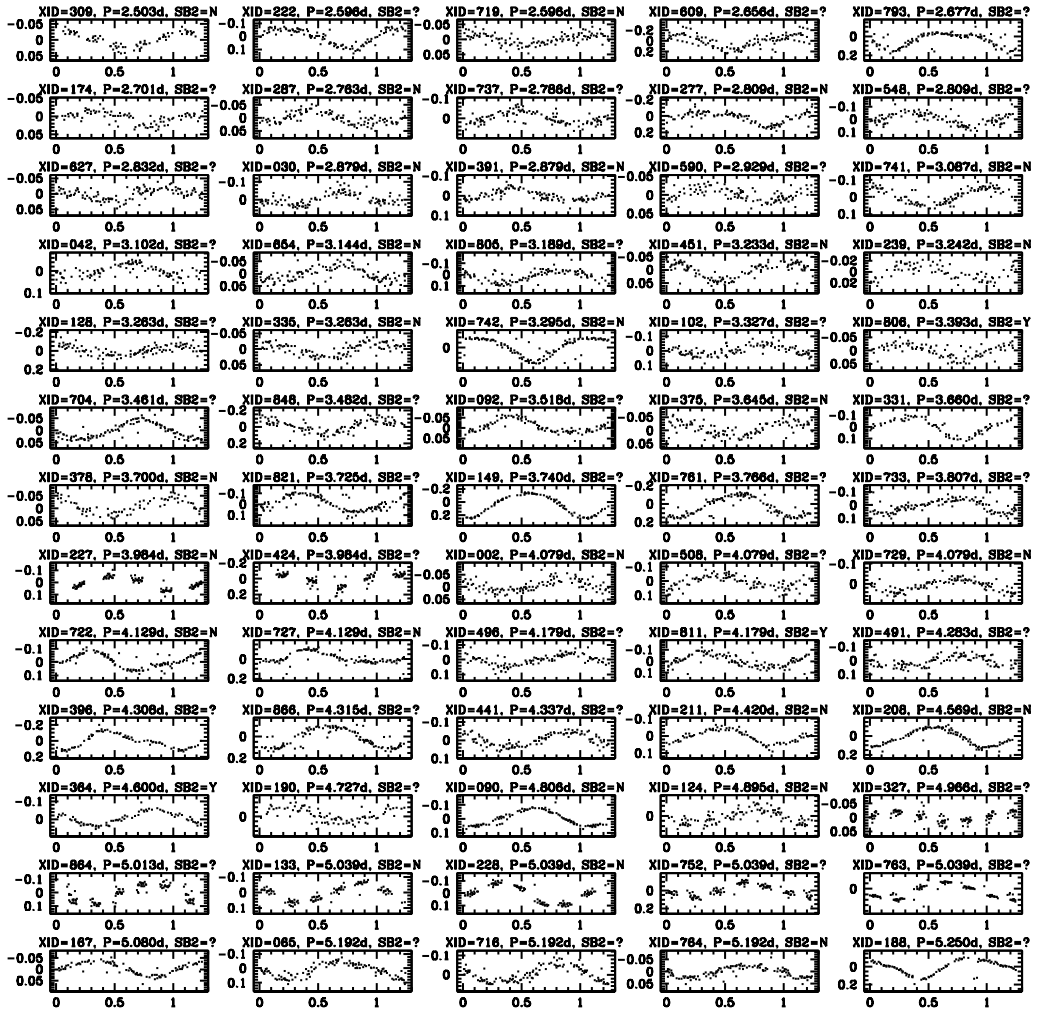


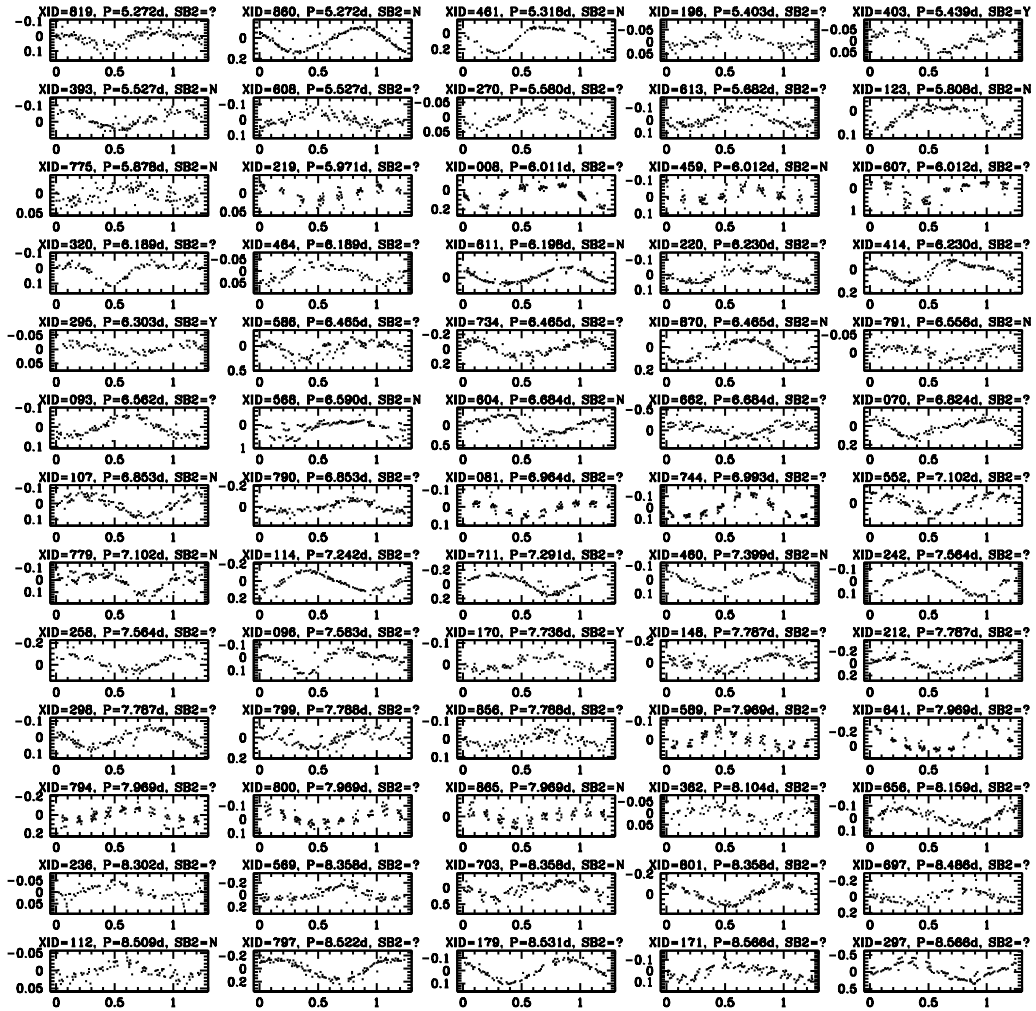
FIG. 4.— Light curves of NGC 6530 cluster members with “definite” rotation periods (FAP ≤ 0.001). The light curves are folded on the derived rotation period (shown above each light curve) and replicated over an additional 0.25 phase for clarity. Also shown above each light curve is the ID number from the X-ray study of Damiani et al. (2004), as well as a flag indicating whether previous spectroscopic observations suggest the star is a spectroscopic binary (SB2). The stars are shown ordered by increasing period.

Differential I Magnitude



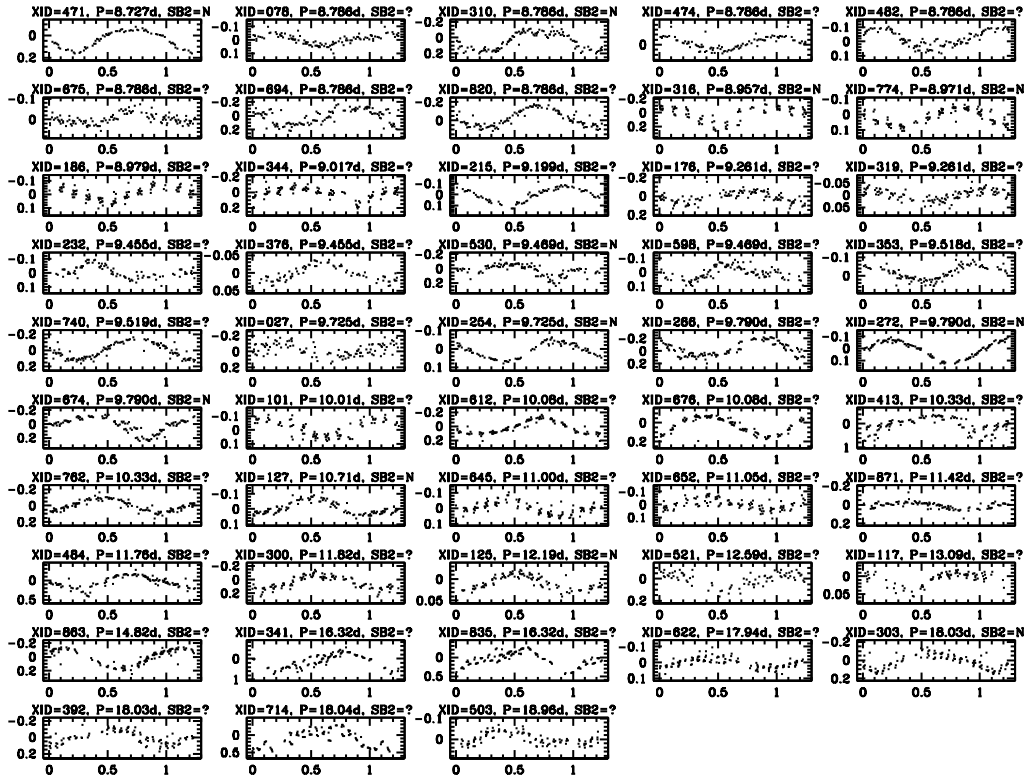
Phase

Differential I Magnitude



Phase

Differential I Magnitude



Phase

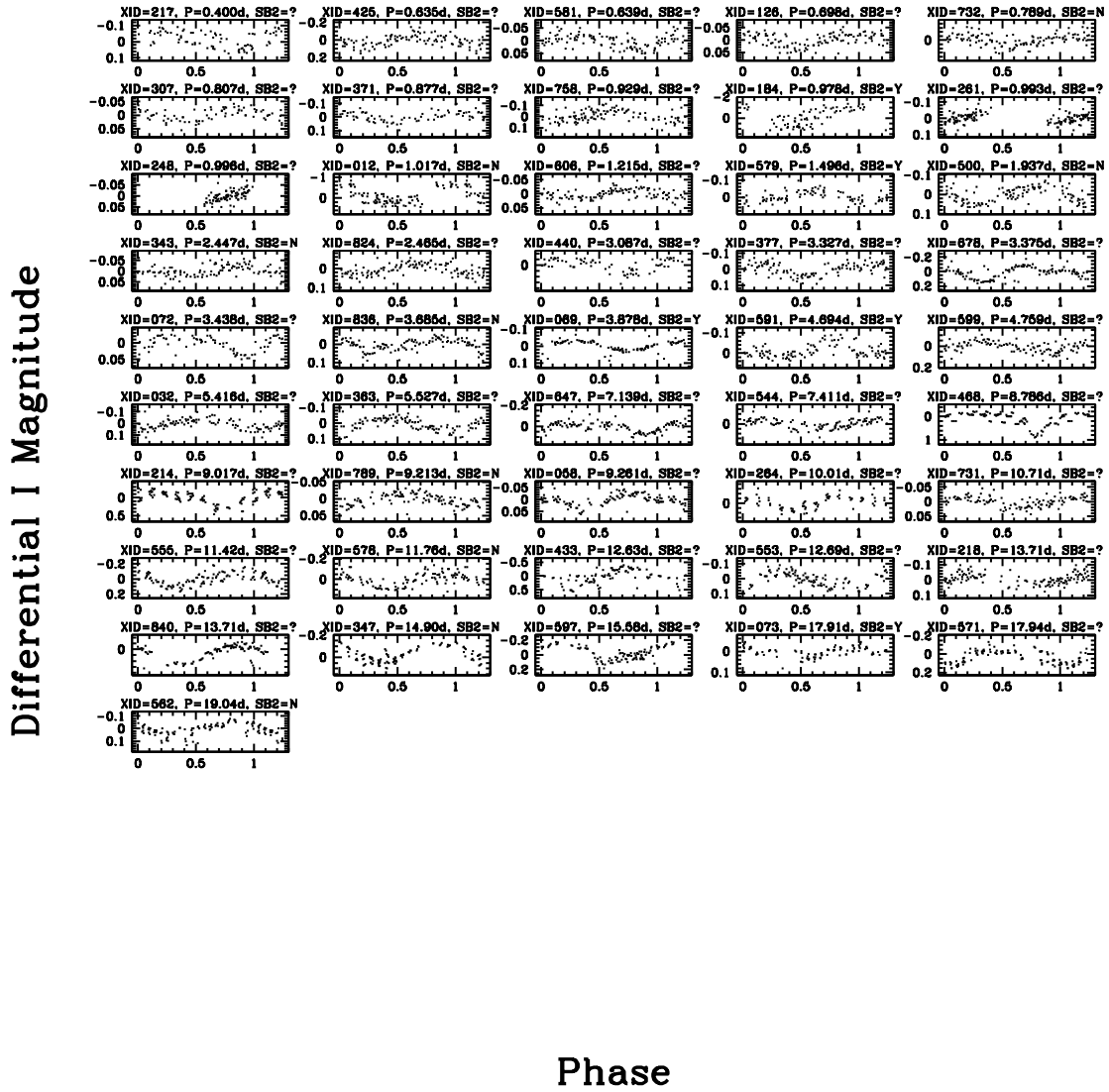


FIG. 5.— Same as Fig. 4 but for NGC 6530 cluster members with “possible” rotation periods ($0.001 < \text{FAP} \leq 0.01$).

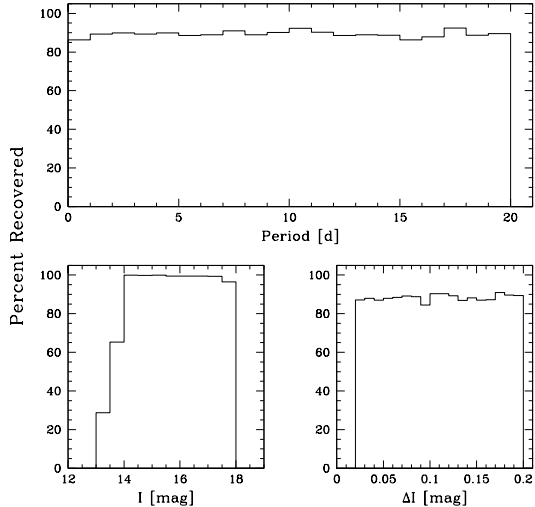


FIG. 6.— Efficiency of period detection. (*Top:* This figure shows the fraction of correctly detected periods as a function of input period, using as a control our light curves of non-variable stars spanning the same range of I_C magnitudes as our sample of rotators. We inject sinusoids with amplitudes in the range $0.02 \leq \Delta I \leq 0.2$ mag into the light curves, and consider the period successfully recovered if it matches the input period to within 10%. (*Bottom left:*) Same as top panel, but showing period recovery fraction as a function of I_C magnitude. (*Bottom right:*) Same as other panels, but showing period recovery fraction as a function of injected amplitude.

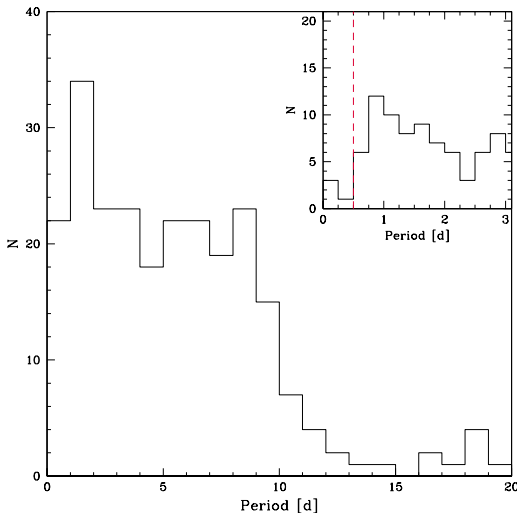


FIG. 7.— The period distribution of our sample of 244 definite NGC 6530 rotators, with bins of 1 d. The inset shows the same distribution, but with 0.25 d bins at the short-period end of the distribution. The vertical line in the inset shows approximately the rotation period corresponding to breakup speed for the typical rotator in our sample.

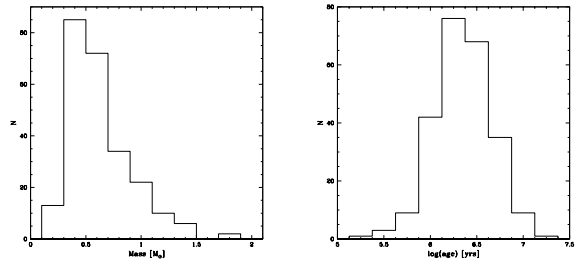


FIG. 8.— Distributions of masses (left) and ages (right) for our sample of NGC 6530 cluster members with rotation periods (see Fig. 7). Masses and ages are inferred from the PMS evolutionary tracks of Siess et al. (2000).

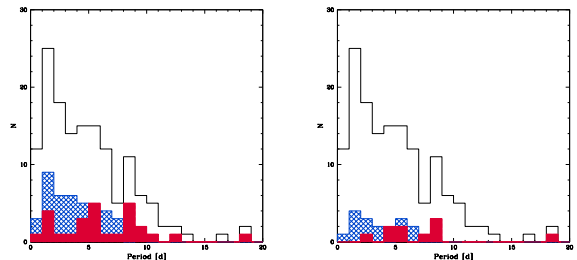


FIG. 9.— *Left:* Rotation period distributions of NGC 6530 cluster members exhibiting NIR excess emission indicative of disks (shaded red histogram) and those that do not exhibit NIR excess emission (hatched blue histogram), as determined via the Q_{VIJK} index (Damiani et al. 2006). A KS test and a Student’s t test both indicate that distributions of NIR excess stars vs. non-excess stars are statistically different, with the NIR excess stars rotating more slowly on average (see Table 6). *Right:* Rotation period distributions of NGC 6530 cluster members classified as CTTs (red) and WTTs (blue) based on strength of $H\alpha$ emission (Prisinzano et al. 2007; Arias et al. 2007). A KS test and a Student’s t test both indicate that distributions of CTTs vs. WTTs are statistically different, with the CTTs rotating more slowly on average (see Table 6). In both panels the open (black) histogram shows the rotation period distribution for the entire sample (see Fig. 7), but including only “high mass” stars with $M_* > 0.5 M_\odot$ because the NIR excess and T Tauri star samples are observationally biased against low masses (see text).

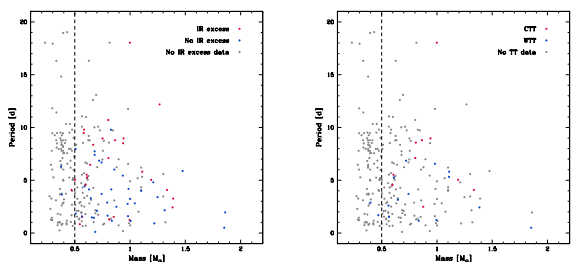


FIG. 10.— Period vs. mass for our sample of NGC 6530 rotators. (*Left:*) Red points are those stars identified as having NIR excess as measured via the Q_{VIJK} index (Damiani et al. 2006), blue points are those with no NIR excess, and gray points are the remainder of the sample (no NIR classification). (*Right:*) Red points are those stars identified as CTTs, blue points are WTTs (Prisinzano et al. 2007; Arias et al. 2007), and gray points are the remainder of the sample (no $H\alpha$ spectrum available). In both panels, the dashed vertical line demarcates the two mass bins we use for statistically comparing the period distribution as a function of stellar mass. A KS test and a Student’s t test both reveal a statistically significant tendency for the lower mass stars to rotate more slowly on average than the higher mass stars (see Table 6).

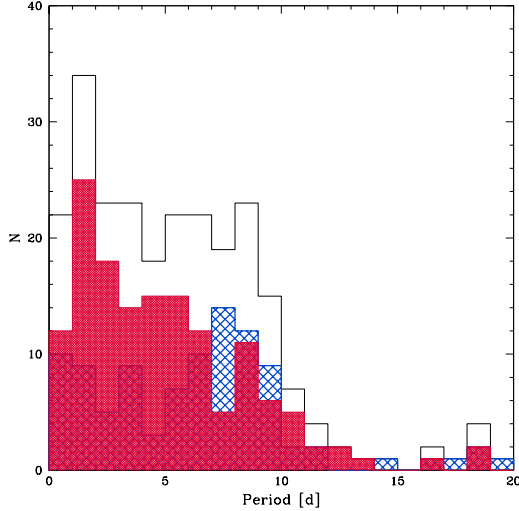


FIG. 11.— Comparison of the rotation period distributions for “high mass” and “low mass” stars in our sample of NGC 6530 rotators. The red shaded histogram represents stars with $M_* > 0.5 M_\odot$ and the blue hatched histogram represents stars $M_* \leq 0.5 M_\odot$. A KS test and a Student’s t test both indicate strong statistical differences between the rotation periods of the high-mass and low-mass stars, with the high-mass stars rotating faster on average (see Table 6).

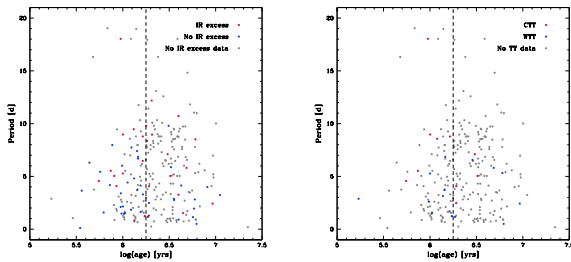


FIG. 12.— Period vs. age for our sample of NGC 6530 rotators. (*Left:*) Red points are those stars identified as having NIR excess as measured via the Q_{VIJK} index (Damiani et al. 2006), blue points are those with no NIR excess, and gray points are those with no NIR classification. (*Right:*) Red points are those stars identified as CTTs, blue points are WTTSs (Prisinzano et al. 2007; Arias et al. 2007), and gray points are those with no $H\alpha$ spectrum. In both panels, the dashed vertical line demarcates the two age bins used in our comparison of “old” vs. “young” stars. A KS test suggests a mild tendency for the younger stars to rotate more rapidly on average (see Table 6).

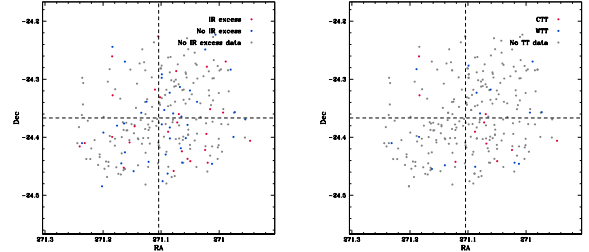


FIG. 13.— The spatial distribution of our sample of NGC 6530 rotators. (*Left:*) Red points are those stars identified as having NIR excess in the Q_{VIJK} index (Damiani et al. 2006), blue points are those with no NIR excess, and gray points are those with no NIR classification. (*Right:*) Red points are those stars identified as CTTs, blue points are WTTSs (Prisinzano et al. 2007; Arias et al. 2007), and gray points are those with no $H\alpha$ spectrum. In both panels, the dashed lines demarcate the quadrants that we use to investigate gradients in age and rotation within the cluster (see also Damiani et al. 2004). A KS test suggests a potential southeast–northwest gradient in the rotation periods.

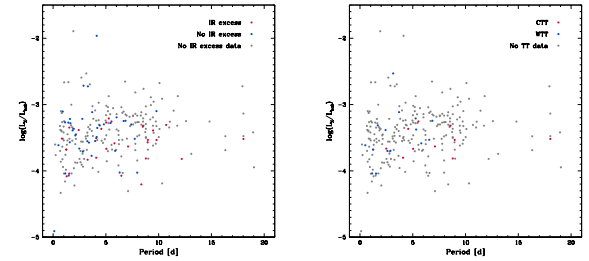


FIG. 14.— L_X/L_{bol} vs. rotation period for our sample of rotators in NGC 6530. (*Left:*) Red points are those stars identified as having NIR excess in the Q_{VIJK} index (Damiani et al. 2006), blue points are those with no NIR excess, and gray points are those with no NIR classification. (*Right:*) Red points are those stars identified as CTTs, blue points are WTTSs (Prisinzano et al. 2007; Arias et al. 2007), and gray points are those with no $H\alpha$ spectrum. A KS test and a Student’s t test both show a statistically significant tendency for the most rapidly rotating stars to have lower L_X/L_{bol} (see Table 7), suggestive of so-called “super-saturation” (e.g. James et al. 2000).

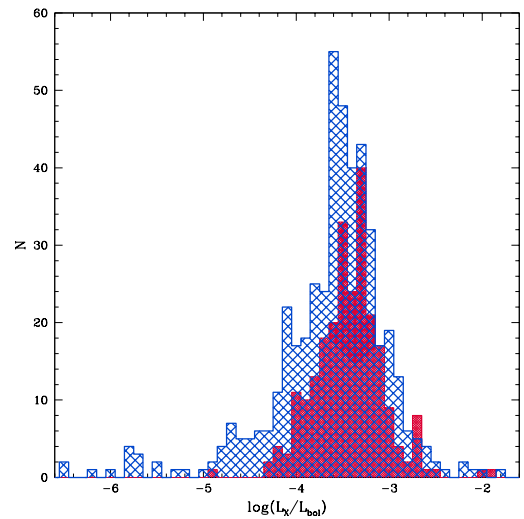


FIG. 15.— The red shaded histogram represents L_X/L_{bol} for NGC 6530 stars with rotation periods, and the blue hatched histogram represents L_X/L_{bol} for those without rotation periods. Stars with rotation periods have significantly higher L_X/L_{bol} on average than those without detected periods (see Table 7).

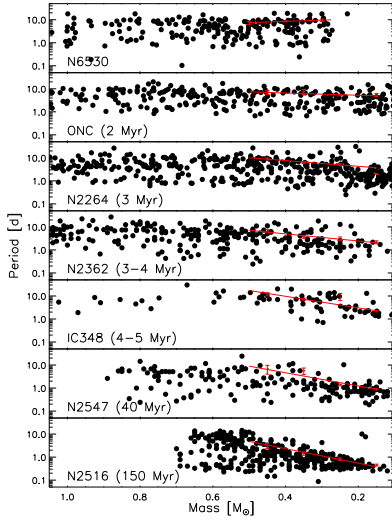


FIG. 16.— Rotation period as a function of mass for (top to bottom): NGC 6530, the ONC, NGC 2264, NGC 2362, IC 348, NGC 2547, and NGC 2516. Periods and masses for all clusters except NGC 6530 and IC 348 are from the compilation of Irwin et al. (2008a), with masses determined via interpolation on the PMS evolutionary tracks of Siess et al. (2000). Periods for IC 348 are from Cieza & Baliber (2006) and we derived masses using data from that paper by interpolating on the Siess et al. (2000) tracks. Periods and masses for NGC 6530 are from the present study. Solid lines in each panel represent a least-squares fit to the 75%-ile upper envelope of periods in each $0.1\text{-}M_{\odot}$ mass bin for masses in the range $0.1\text{--}0.5 M_{\odot}$, except for NGC 6530 which is limited to the range $0.2\text{--}0.5 M_{\odot}$ (see §5 for discussion of this figure).

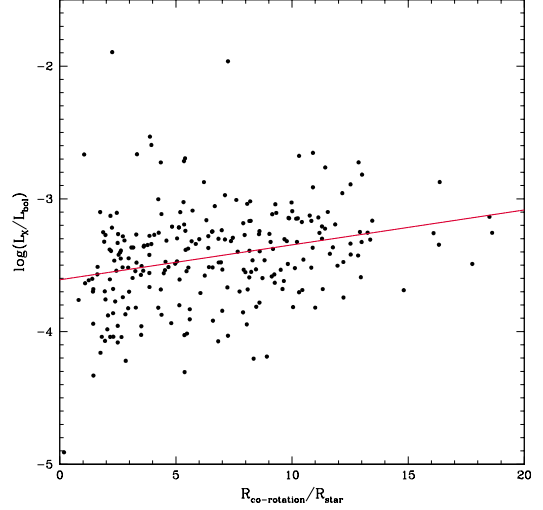


FIG. 18.— $\log(L_X/L_{\text{bol}})$ vs. $R_{\text{co-rotation}}/R_{\star}$ for NGC 6530 stars with rotation periods. The line represents a linear best fit of the form $\log(L_X/L_{\text{bol}}) = 0.026(\pm 0.006) \times R_{\text{co-rotation}}/R_{\star} - 3.61(\pm 0.05)$. A Kendall's τ test shows the trend to be highly statistically significant. This suggests that centrifugal stripping of the stellar corae may be responsible for the super-saturation effect observed in Fig. 14 (see also Wright et al. 2011).

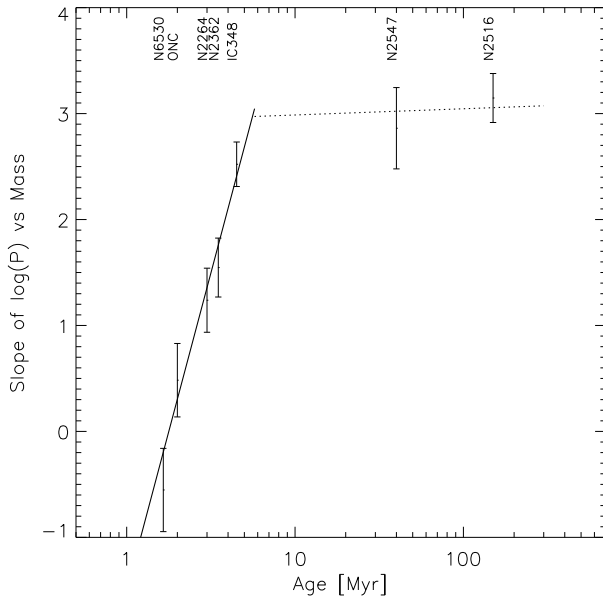


FIG. 17.— Slopes of the mass–period relationships from Fig. 16 versus cluster age. Cluster ages are from Mayne et al. (2007) and Mayne & Naylor (2008), except for NGC 6530 whose age was adjusted here to be consistent with the linear relationship (solid line) fitted to the ONC, NGC 2264, NGC 2362, and IC 348. The maximum age inferred for NGC 6530 is 1.65 Myr, on an age scale where the ONC is 2 Myr. See §5 for discussion of this figure.

REFERENCES

- Aarnio, A. N., Stassun, K. G., Hughes, W. J., & McGregor, S. L. 2011, *Sol. Phys.*, 268, 195
- Aarnio, A. N., Stassun, K. G., & Matt, S. P. 2009, in *American Institute of Physics Conference Series*, Vol. 1094, American Institute of Physics Conference Series, ed. E. Stempels, 337–340
- Aarnio, A. N., Stassun, K. G., & Matt, S. P. 2010, *ApJ*, 717, 93
- Allain, S., Bouvier, J., Prosser, C., Marschall, L. A., & Laaksonen, B. D. 1996, *A&A*, 305, 498
- Arias, J. I., Barbá, R. H., & Morrell, N. I. 2007, *MNRAS*, 374, 1253
- Aspin, C. 2011, *AJ*, 142, 135
- Aspin, C., Barbieri, C., Boschi, F., Di Mille, F., Rampazzi, F., Reipurth, B., & Tsvetkov, M. 2006, *AJ*, 132, 1298
- Attridge, J. M. & Herbst, W. 1992, *ApJ*, 398, L61
- Barnes, S. A. 2003, *ApJ*, 586, 464
- . 2007, *ApJ*, 669, 1167
- . 2010, *ApJ*, 722, 222
- Barnes, S. A. & Kim, Y.-C. 2010, *ApJ*, 721, 675
- Barnes, S. A., Sofia, S., Prosser, C. F., & Stauffer, J. R. 1999, *ApJ*, 516, 263
- Basri, G., Johns-Krull, C. M., & Mathieu, R. D. 1997, *AJ*, 114, 781
- Bastien, F. A., Stassun, K. G., & Weintraub, D. A. 2011, *AJ*, 142, 141
- Bouvier, J., Alencar, S. H. P., Harries, T. J., Johns-Krull, C. M., & Romanova, M. M. 2007, *Protostars and Planets V*, 479
- Bouvier, J., Bertout, C., Benz, W., & Mayor, M. 1986, *A&A*, 165, 110
- Bouvier, J., Cabrit, S., Fernandez, M., Martin, E. L., & Matthews, J. M. 1993, *A&A*, 272, 176
- Bouvier, J., Chelli, A., Allain, S., Carrasco, L., Costero, R., Cruz-Gonzalez, I., Dougados, C., Fernández, M., Martín, E. L., Ménaud, F., Mennessier, C., Mujica, R., Recillas, E., Salas, L., Schmidt, G., & Wichmann, R. 1999, *A&A*, 349, 619
- Bouvier, J., Dougados, C., & Alencar, S. H. P. 2004, *Ap&SS*, 292, 659
- Bouvier, J., Grankin, K. N., Alencar, S. H. P., Dougados, C., Fernández, M., Basri, G., Batalha, C., Guenther, E., Ibrahimov, M. A., Magakian, T. Y., Melnikov, S. Y., Petrov, P. P., Rud, M. V., & Zapatero Osorio, M. R. 2003, *A&A*, 409, 169
- Bouvier, J., Wichmann, R., Grankin, K., Allain, S., Covino, E., Fernandez, M., Martin, E. L., Terranegra, L., Catalano, S., & Marilli, E. 1997, *A&A*, 318, 495
- Briceño, C., Vivas, A. K., Hernández, J., Calvet, N., Hartmann, L., Megeath, T., Berlind, P., Calkins, M., & Hoyer, S. 2004, *ApJ*, 606, L123
- Casey, B. W., Mathieu, R. D., Vaz, L. P. R., Andersen, J., & Suntzeff, N. B. 1998, *AJ*, 115, 1617
- Choi, P. I. & Herbst, W. 1996, *AJ*, 111, 283
- Cieza, L. & Baliber, N. 2006, *ApJ*, 649, 862
- Covey, K. R., Hillenbrand, L. A., Miller, A. A., Poznanski, D., Cenko, S. B., Silverman, J. M., Bloom, J. S., Kasliwal, M. M., Fischer, W., Rayner, J., Rebull, L. M., Butler, N. R., Filippenko, A. V., Law, N. M., Ofek, E. O., Agüeros, M., Dekany, R. G., Rahmer, G., Hale, D., Smith, R., Quimby, R. M., Nugent, P., Jacobsen, J., Zolkower, J., Velur, V., Walters, R., Henning, J., Bui, K., McKenna, D., Kulkarni, S. R., & Klein, C. 2011, *AJ*, 141, 40
- Covino, E., Catalano, S., Frasca, A., Marilli, E., Fernández, M., Alcalá, J. M., Melo, C., Paladino, R., Sterzik, M. F., & Stelzer, B. 2000, *A&A*, 361, L49
- Da Rio, N., Robberto, M., Soderblom, D. R., Panagia, N., Hillenbrand, L. A., Palla, F., & Stassun, K. G. 2010, *ApJ*, 722, 1092
- Damiani, F., Flaccomio, E., Micela, G., Sciortino, S., Harnden, Jr., F. R., & Murray, S. S. 2004, *ApJ*, 608, 781
- Damiani, F., Prisinzano, L., Micela, G., & Sciortino, S. 2006, *A&A*, 459, 477
- Favata, F., Flaccomio, E., Reale, F., Micela, G., Sciortino, S., Shang, H., Stassun, K. G., & Feigelson, E. D. 2005, *ApJS*, 160, 469
- Feigelson, E., Townsley, L., Güdel, M., & Stassun, K. 2007, *Protostars and Planets V*, 313
- Feigelson, E. D., Garmire, G. P., & Pravdo, S. H. 2002, *ApJ*, 572, 335
- Feigelson, E. D., Getman, K., Townsley, L., Garmire, G., Preibisch, T., Grosso, N., Montmerle, T., Muench, A., & McCaughrean, M. 2005, *ApJS*, 160, 379
- Feigelson, E. D., Getman, K. V., Townsley, L. K., Broos, P. S., Povich, M. S., Garmire, G. P., King, R. R., Montmerle, T., Preibisch, T., Smith, N., Stassun, K. G., Wang, J., Wolk, S., & Zinnecker, H. 2011, *ApJS*, 194, 9
- Getman, K. V., Feigelson, E. D., Grosso, N., McCaughrean, M. J., Micela, G., Broos, P., Garmire, G., & Townsley, L. 2005a, *ApJS*, 160, 353
- Getman, K. V., Flaccomio, E., Broos, P. S., Grosso, N., Tsujimoto, M., Townsley, L., Garmire, G. P., Kastner, J., Li, J., Harnden, Jr., F. R., Wolk, S., Murray, S. S., Lada, C. J., Muench, A. A., McCaughrean, M. J., Meeus, G., Damiani, F., Micela, G., Sciortino, S., Bally, J., Hillenbrand, L. A., Herbst, W., Preibisch, T., & Feigelson, E. D. 2005b, *ApJS*, 160, 319
- Gómez Maqueo Chew, Y., Stassun, K. G., Prša, A., & Mathieu, R. D. 2009, *ApJ*, 699, 1196
- Grosso, N., Feigelson, E. D., Getman, K. V., Townsley, L., Broos, P., Flaccomio, E., McCaughrean, M. J., Micela, G., Sciortino, S., Bally, J., Smith, N., Muench, A. A., Garmire, G. P., & Palla, F. 2005, *ApJS*, 160, 530
- Güdel, M., Briggs, K. R., Arzner, K., Audard, M., Bouvier, J., Feigelson, E. D., Franciosini, E., Glauser, A., Grosso, N., Micela, G., Monin, J.-L., Montmerle, T., Padgett, D. L., Palla, F., Pillitteri, I., Rebull, L., Scelsi, L., Silva, B., Skinner, S. L., Stelzer, B., & Telleschi, A. 2007, *A&A*, 468, 353
- Guenther, D. B., Kallinger, T., Zwintz, K., Weiss, W. W., & Tanner, J. 2007, *ApJ*, 671, 581
- Gullbring, E. & Gahm, G. F. 1996, *A&A*, 308, 821
- Güver, T. & Özel, F. 2009, *MNRAS*, 400, 2050
- Hartman, J. D., Gaudi, B. S., Holman, M. J., McLeod, B. A., Stanek, K. Z., Barranco, J. A., Pinsonneault, M. H., & Kalirai, J. S. 2008, *ApJ*, 675, 1254
- Hartmann, L., Hewett, R., Stahler, S., & Mathieu, R. D. 1986, *ApJ*, 309, 275
- Hebb, L., Stempels, H. C., Aigrain, S., Collier-Cameron, A., Hodgkin, S. T., Irwin, J. M., Maxted, P. F. L., Pollacco, D., Street, R. A., Wilson, D. M., & Stassun, K. G. 2010, *A&A*, 522, A37+
- Herbst, W., Bailer-Jones, C. A. L., & Mundt, R. 2001, *ApJ*, 554, L197
- Herbst, W., Bailer-Jones, C. A. L., Mundt, R., Meisenheimer, K., & Wackermann, R. 2002, *A&A*, 396, 513
- Herbst, W., Eislöffel, J., Mundt, R., & Scholz, A. 2007, *Protostars and Planets V*, 297
- Herbst, W., Hamilton, C. M., Leduc, K., Winn, J. N., Johns-Krull, C. M., Mundt, R., & Ibrahimov, M. 2008, *Nature*, 452, 194
- Herbst, W., Herbst, D. K., Grossman, E. J., & Weinstein, D. 1994, *AJ*, 108, 1906
- Herbst, W., LeDuc, K., Hamilton, C. M., Winn, J. N., Ibrahimov, M., Mundt, R., & Johns-Krull, C. M. 2010, *AJ*, 140, 2025
- Herbst, W., Maley, J. A., & Williams, E. C. 2000, *AJ*, 120, 349
- Hillenbrand, L. A. 1997, *AJ*, 113, 1733
- Honeycutt, R. K. 1992, *PASP*, 104, 435
- Irwin, J., Aigrain, S., Hodgkin, S., Stassun, K. G., Hebb, L., Irwin, M., Moraux, E., Bouvier, J., Alapini, A., Alexander, R., Bramich, D. M., Holtzman, J., Martín, E. L., McCaughrean, M. J., Pont, F., Verrier, P. E., & Zapatero Osorio, M. R. 2007, *MNRAS*, 380, 541
- Irwin, J., Hodgkin, S., Aigrain, S., Bouvier, J., Hebb, L., Irwin, M., & Moraux, E. 2008a, *MNRAS*, 384, 675
- Irwin, J., Hodgkin, S., Aigrain, S., Bouvier, J., Hebb, L., & Moraux, E. 2008b, *MNRAS*, 383, 1588
- James, D. J., Jardine, M. M., Jeffries, R. D., Randich, S., Collier Cameron, A., & Ferreira, M. 2000, *MNRAS*, 318, 1217
- Jensen, E. L. N., Dhital, S., Stassun, K. G., Patience, J., Herbst, W., Walter, F. M., Simon, M., & Basri, G. 2007, *AJ*, 134, 241
- Kastner, J. H., Richmond, M., Grosso, N., Weintraub, D. A., Simon, T., Frank, A., Hamaguchi, K., Ozawa, H., & Henden, A. 2004, *Nature*, 430, 429
- Kearns, K. E., Eaton, N. L., Herbst, W., & Mazzurco, C. J. 1997, *AJ*, 114, 1098
- Kearns, K. E. & Herbst, W. 1998, *AJ*, 116, 261

- Kenyon, S. J. & Hartmann, L. 1995, *ApJS*, 101, 117
- Koenigl, A. 1991, *ApJ*, 370, L39
- Krishnamurthi, A., Terndrup, D. M., Pinsonneault, M. H., Sellgren, K., Stauffer, J. R., Schild, R., Backman, D. E., Beisser, K. B., Dahari, D. B., Dasgupta, A., Hagelgans, J. T., Seeds, M. A., Anand, R., Laaksonen, B. D., Marschall, L. A., & Ramseyer, T. 1998, *ApJ*, 493, 914
- Lada, C. J., Gottlieb, C. A., Gottlieb, E. W., & Gull, T. R. 1976, *ApJ*, 203, 159
- Lamm, M. H., Mundt, R., Bailer-Jones, C. A. L., & Herbst, W. 2005, *A&A*, 430, 1005
- Lang, D., Hogg, D. W., Mierle, K., Blanton, M., & Roweis, S. 2010, *AJ*, 139, 1782
- Le Blanc, T. S., Covey, K. R., & Stassun, K. G. 2011, *ArXiv e-prints*
- Loktin, A., Zakharova, P., Gerasimenko, T., & Malisheva, L. 1997, *Baltic Astronomy*, 6, 316
- Lomb, N. R. 1976, *Ap&SS*, 39, 447
- Makidon, R. B., Rebull, L. M., Strom, S. E., Adams, M. T., & Patten, B. M. 2004, *AJ*, 127, 2228
- Mathieu, R. D., Stassun, K., Basri, G., Jensen, E. L. N., Johns-Krull, C. M., Valenti, J. A., & Hartmann, L. W. 1997, *AJ*, 113, 1841
- Matt, S. & Pudritz, R. E. 2004, *ApJ*, 607, L43
- 2005a, *ApJ*, 632, L135
- 2005b, *MNRAS*, 356, 167
- 2008a, *ApJ*, 678, 1109
- 2008b, *ApJ*, 681, 391
- Mayne, N. J. & Naylor, T. 2008, *MNRAS*, 386, 261
- Mayne, N. J., Naylor, T., Littlefair, S. P., Saunders, E. S., & Jeffries, R. D. 2007, *MNRAS*, 375, 1220
- Menten, K. M., Reid, M. J., Forbrich, J., & Brunthaler, A. 2007, *A&A*, 474, 515
- Mohanty, S., Stassun, K. G., & Doppmann, G. W. 2010, *ApJ*, 722, 1138
- Mohanty, S., Stassun, K. G., & Mathieu, R. D. 2009, *ApJ*, 697, 713
- Najita, J. 1995, in *Revista Mexicana de Astronomia y Astrofisica*, vol. 27, Vol. 1, *Revista Mexicana de Astronomia y Astrofisica Conference Series*, ed. S. Lizano & J. M. Torrelles, 293–+
- Ostriker, E. C. & Shu, F. H. 1995, *ApJ*, 447, 813
- Patten, B. M. & Simon, T. 1996, *ApJS*, 106, 489
- Pizzolato, N., Maggio, A., Micela, G., Sciortino, S., & Ventura, P. 2003, *A&A*, 397, 147
- Press, W. H. & Rybicki, G. B. 1989, *ApJ*, 338, 277
- Press, W. H., Teukolsky, S. A., Vetterling, W. T., & Flannery, B. P. 1992, *Numerical recipes in C. The art of scientific computing*, ed. Press, W. H., Teukolsky, S. A., Vetterling, W. T., & Flannery, B. P.
- Prisinzano, L., Damiani, F., Micela, G., & Pillitteri, I. 2007, *A&A*, 462, 123
- Prisinzano, L., Damiani, F., Micela, G., & Sciortino, S. 2005, *A&A*, 430, 941
- Radick, R. R., Skiff, B. A., & Lockwood, G. W. 1990, *ApJ*, 353, 524
- Radick, R. R., Thompson, D. T., Lockwood, G. W., Duncan, D. K., & Baggett, W. E. 1987, *ApJ*, 321, 459
- Rebull, L. M. 2001, *AJ*, 121, 1676
- Scargle, J. D. 1982, *ApJ*, 263, 835
- Shu, F., Najita, J., Ostriker, E., Wilkin, F., Ruden, S., & Lizano, S. 1994, *ApJ*, 429, 781
- Siess, L., Dufour, E., & Forestini, M. 2000, *A&A*, 358, 593
- Stassun, K. & Wood, K. 1999, *ApJ*, 510, 892
- Stassun, K. G., Ardila, D. R., Barsony, M., Basri, G., & Mathieu, R. D. 2004a, *AJ*, 127, 3537
- Stassun, K. G., Hebb, L., López-Morales, M., & Prša, A. 2009, in *IAU Symposium*, Vol. 258, *IAU Symposium*, ed. E. E. Mamajek, D. R. Soderblom, & R. F. G. Wyse, 161–170
- Stassun, K. G., Mathieu, R. D., Cargile, P. A., Aarnio, A. N., Stempels, E., & Geller, A. 2008, *Nature*, 453, 1079
- Stassun, K. G., Mathieu, R. D., Mazeh, T., & Vrba, F. J. 1999, *AJ*, 117, 2941
- Stassun, K. G., Mathieu, R. D., & Valenti, J. A. 2006a, *Nature*, 440, 311
- 2007a, *ApJ*, 664, 1154
- Stassun, K. G., Mathieu, R. D., Vaz, L. P. R., Stroud, N., & Vrba, F. J. 2004b, *ApJS*, 151, 357
- Stassun, K. G., Mathieu, R. D., Vrba, F. J., Mazeh, T., & Henden, A. 2001, *AJ*, 121, 1003
- Stassun, K. G. & Terndrup, D. 2003, *PASP*, 115, 505
- Stassun, K. G., van den Berg, M., & Feigelson, E. 2007b, *ApJ*, 660, 704
- Stassun, K. G., van den Berg, M., Feigelson, E., & Flaccomio, E. 2006b, *ApJ*, 649, 914
- Stassun, K. G., van den Berg, M., Mathieu, R. D., & Verbunt, F. 2002, *A&A*, 382, 899
- Stauffer, J. R. & Hartmann, L. W. 1987, *ApJ*, 318, 337
- Stempels, H. C., Hebb, L., Stassun, K. G., Holtzman, J., Dunstone, N., Glowienka, L., & Frandsen, S. 2008, *A&A*, 481, 747
- Sung, H., Chun, M.-Y., & Bessell, M. S. 2000, *AJ*, 120, 333
- van den Ancker, M. E., The, P. S., Feinstein, A., Vazquez, R. A., de Winter, D., & Perez, M. R. 1997, *A&AS*, 123, 63
- van Eyken, J. C., Ciardi, D. R., Rebull, L. M., Stauffer, J. R., Akeson, R. L., Beichman, C. A., Boden, A. F., von Braun, K., Gelino, D. M., Hoard, D. W., Howell, S. B., Kane, S. R., Plavchan, P., Ramírez, S. V., Bloom, J. S., Cenko, S. B., Kasliwal, M. M., Kulkarni, S. R., Law, N. M., Nugent, P. E., Ofek, E. O., Poznanski, D., Quimby, R. M., Grillmair, C. J., Laher, R., Levitan, D., Mattingly, S., & Surace, J. A. 2011, *AJ*, 142, 60
- Vogel, S. N. & Kuhl, L. V. 1981, *ApJ*, 245, 960
- Walter, F. M., Neff, J. E., Gibson, D. M., Linsky, J. L., Rodono, M., Gary, D. E., & Butler, C. J. 1987, *A&A*, 186, 241
- Walter, F. M., Stringfellow, G. S., Sherry, W. H., & Field-Pollatou, A. 2004, *AJ*, 128, 1872
- Winn, J. N., Hamilton, C. M., Herbst, W. J., Hoffman, J. L., Holman, M. J., Johnson, J. A., & Kuchner, M. J. 2006, *ApJ*, 644, 510
- Wright, N. J., Drake, J. J., Mamajek, E. E., & Henry, G. W. 2011, *ArXiv e-prints*
- Zwintz, K. & Weiss, W. W. 2006, *A&A*, 457, 237

TABLE 1
ALL OBSERVATIONAL DATA

Season	Telescope	Nights of Data
June–July 2004	CTIO 0.9m	12
July 2005	CTIO 1.0m	6
June–July 2006	CTIO 1.0m	27
June–July 2007	CTIO 1.0m	15
April 2008	CTIO 1.0m	8
May–June 2009	CTIO 1.0m	20

TABLE 2
2006 SEASON DATA

Field	α_{2000} [hh mm ss.s]	δ_{2000} [dd mm ss]	Exp Time [s]	No. of Frames
1	18 05 01.6	-24 12 34	720	97
2	18 05 01.6	-24 29 34	720	95
3	18 03 46.9	-24 29 34	720	90
4	18 03 46.9	-24 12 34	720	85

TABLE 3
X-RAY POSITIONAL
OFFSETS

Field	Δ RA	Δ DEC
1	0.20''	0.45''
2	0.00''	0.15''
3	-0.30''	-0.15''
4	-1.05''	-0.20''

TABLE 4
PARAMETERS OF THE 244 CLUSTER MEMBERS WITH DEFINITE ROTATION PERIODS

ID X-ray	ID WFI	RA [deg]	DEC [deg]	V [mag]	I [mag]	Period [d]	Mass [M_{\odot}]	Age [Myrs]	L_{bol} [L_{\odot}]	Radius [R_{\odot}]	$\log(L_X)$ [erg s^{-1}]	IR excess?	H α class? ^a	SB2?
423	14403	271.09209	-24.42964	15.692	13.557	0.10352	0.69	0.35	5.12	4.49	29.382	N	-	N
138	27470	271.02700	-24.29480	17.948	16.261	0.18743	0.94	22.23	0.39	0.96	29.566	-	-	N
067	28743	270.99692	-24.28292	19.389	16.527	0.24286	0.36	2.02	0.32	1.44	29.331	-	-	N
024	21464	270.97288	-24.35667	14.522	13.271	0.49948	1.85	6.22	7.02	2.61	30.815	N	W	N
040	25374	270.98342	-24.32083	18.483	16.215	0.65205	0.57	3.00	0.43	1.37	29.895	-	-	-
537	34984	271.11225	-24.23632	18.248	15.843	0.66582	0.48	1.44	0.62	1.76	29.675	-	-	-
357	26832	271.08246	-24.30170	18.544	16.315	0.68347	0.60	3.81	0.39	1.28	29.794	-	-	-
130	15487	271.02346	-24.41538	16.420	14.548	0.71534	1.00	1.33	1.85	2.32	29.518	-	-	-
175	13073	271.03913	-24.45115	17.667	15.693	0.72441	0.90	4.51	0.63	1.43	29.523	-	-	Y
075	16658	271.00055	-24.40260	19.647	16.647	0.73687	0.34	2.17	0.29	1.38	29.941	-	-	-
329	25964	271.07742	-24.31265	19.637	16.924	0.77710	0.38	3.29	0.23	1.17	29.546	-	-	-
055	22050	270.99275	-24.35137	18.154	16.064	0.80087	0.76	5.15	0.45	1.27	29.834	-	-	-
080	15298	271.00225	-24.41743	19.202	16.687	0.81196	0.43	2.92	0.29	1.26	29.917	-	-	-
273	14748	271.06417	-24.42415	17.859	15.569	0.83572	0.55	1.34	0.78	1.88	29.962	Y	-	Y
324	23459	271.07588	-24.33860	18.998	16.633	0.85932	0.50	3.78	0.30	1.20	29.796	-	-	-
787	16230	271.18758	-24.40722	18.441	15.772	0.86751	0.39	0.81	1.08	2.56	29.981	-	-	-
108	22808	271.01404	-24.34450	18.264	16.175	0.88178	0.77	6.15	0.41	1.20	29.369	-	-	-
007	20186	270.95492	-24.36911	16.836	15.083	0.90888	1.22	3.99	1.15	1.72	30.536	N	-	N
490	19545	271.10396	-24.37498	17.647	15.738	0.92858	0.99	6.09	0.61	1.36	29.853	-	-	N
632	33389	271.13234	-24.24839	18.121	15.597	0.92888	0.42	1.04	0.78	2.09	29.531	-	-	Y
200	24837	271.04704	-24.32589	20.053	17.090	0.98372	0.35	3.19	0.21	1.15	29.477	-	-	-
842	15133	271.22029	-24.41926	19.734	16.911	0.98467	0.37	3.03	0.23	1.20	29.614	-	-	-
550	22451	271.11551	-24.34757	16.502	14.805	1.01157	1.32	3.25	1.50	1.91	30.217	-	-	-
209	15075	271.04992	-24.41990	18.143	15.987	1.02589	0.67	3.49	0.52	1.41	29.253	-	-	-
074	25071	271.00059	-24.32374	18.286	15.406	1.04408	0.36	0.29	1.36	2.93	31.052	-	-	-
747	24025	271.17030	-24.33339	18.268	15.827	1.04570	0.46	1.37	0.62	1.80	30.125	-	-	-
666	22273	271.14330	-24.34929	17.501	15.242	1.11770	0.56	1.03	1.04	2.13	29.438	-	-	-
720	30485	271.16234	-24.26961	17.567	15.669	1.13633	1.00	5.70	0.65	1.39	30.129	N	-	Y
340	21203	271.07913	-24.35887	17.099	15.111	1.15759	0.83	1.86	1.09	1.90	29.580	N	W	Y
082	13925	271.00259	-24.43722	18.454	15.934	1.16546	0.43	1.36	0.57	1.78	29.582	-	-	-
457	24121	271.09871	-24.33251	20.323	16.972	1.21128	0.30	1.74	0.31	1.56	29.095	-	-	-
778	16987	271.18433	-24.39930	16.652	14.772	1.23261	0.99	1.72	1.50	2.10	30.080	Y	W	N
104	15448	271.01196	-24.41572	20.330	16.813	1.25973	0.28	1.00	0.63	2.23	29.699	-	-	-
495	36379	271.10492	-24.22612	17.184	15.177	1.27958	0.81	1.91	1.02	1.85	29.508	Y	-	N
119	28352	271.01779	-24.28629	17.871	15.571	1.29742	0.54	1.31	0.78	1.89	29.869	-	-	Y
268	16479	271.06263	-24.40452	17.899	15.869	1.35433	0.83	4.82	0.54	1.34	29.769	-	-	Y
318	26918	271.07463	-24.30070	18.503	16.196	1.36147	0.54	2.61	0.44	1.42	29.782	-	-	-
372	16715	271.08480	-24.40194	16.916	14.797	1.43969	0.67	1.03	1.50	2.39	30.488	N	-	Y
111	14269	271.01546	-24.43162	20.785	17.509	1.44576	0.29	3.44	0.16	1.07	30.120	-	-	-
435	21858	271.09446	-24.35300	16.955	14.816	1.47692	0.65	0.97	1.53	2.43	29.698	N	-	Y
057	21369	270.99317	-24.35742	17.507	15.253	1.51950	0.57	1.05	1.02	2.12	29.553	Y	W	N
476	24293	271.10183	-24.33107	17.771	15.765	1.52632	0.85	4.46	0.59	1.40	30.006	Y	-	Y
241	28138	271.05775	-24.28819	18.208	15.876	1.54713	0.52	1.68	0.60	1.68	29.844	-	-	-
458	27805	271.09867	-24.29146	16.822	14.573	1.57578	0.56	0.62	1.93	2.91	30.300	N	-	N
636	21329	271.13421	-24.35777	16.250	14.368	1.59380	0.98	1.05	2.18	2.54	30.704	N	-	Y
131	33362	271.02388	-24.24864	17.040	15.026	1.64049	0.80	1.56	1.17	2.00	30.367	N	-	Y
257	25568	271.06100	-24.31782	18.410	15.983	1.68499	0.47	1.62	0.54	1.66	30.002	-	W ^b	-
098	23688	271.01050	-24.33639	18.271	16.142	1.71903	0.71	4.97	0.43	1.27	30.216	-	-	-
867	20919	271.23655	-24.36153	18.918	16.120	1.74819	0.37	0.86	0.63	2.42	29.509	-	-	-
583	18300	271.12163	-24.38748	18.481	16.248	1.79591	0.60	3.44	0.42	1.33	29.863	-	-	-
304	26297	271.06983	-24.30861	19.720	16.729	1.81047	0.34	2.28	0.28	1.35	29.477	-	-	-
760	19069	271.17596	-24.37997	17.955	15.610	1.84229	0.51	1.23	0.77	1.92	30.077	N	-	N
041	19285	270.98450	-24.37777	17.857	15.727	1.87238	0.69	2.78	0.64	1.56	30.029	-	-	N
064	14711	270.99505	-24.42486	17.279	15.021	1.91422	0.56	0.85	1.26	2.37	31.790	-	-	-
037	28700	270.98017	-24.28335	14.700	13.429	1.94983	1.86	5.85	6.18	2.55	31.007	N	-	Y
430	24720	271.09304	-24.32702	18.243	15.966	1.96745	0.56	2.15	0.54	1.55	29.358	-	-	-
634	15882	271.13296	-24.41119	16.249	14.417	2.01568	1.08	1.29	2.10	2.42	29.685	-	-	-
223	17456	271.05350	-24.39516	18.844	16.499	2.08930	0.52	3.44	0.34	1.26	29.239	-	-	-
679	12608	271.14729	-24.45838	16.647	14.556	2.10225	0.70	0.95	1.83	2.61	30.380	N	-	N
852	19899	271.22629	-24.37153	18.019	15.708	2.10225	0.53	1.48	0.69	1.79	29.828	-	-	-
240	16773	271.05738	-24.40146	15.622	13.898	2.15501	1.31	1.00	3.44	2.93	30.670	N	-	Y
262	17034	271.06175	-24.39890	18.636	16.470	2.15501	0.69	6.76	0.33	1.12	29.582	-	-	-
417	11216	271.09084	-24.47959	20.345	16.760	2.28431	0.28	0.81	0.66	2.30	29.524	-	-	-
049	30517	270.98863	-24.26947	16.317	14.871	2.42001	1.38	9.27	1.47	1.56	30.364	Y	W	N
580	13622	271.12154	-24.44222	17.020	15.059	2.48309	0.88	1.91	1.14	1.91	29.976	N	C	Y
309	29815	271.07129	-24.27430	17.602	15.375	2.50271	0.59	1.23	0.92	1.98	29.726	-	-	N
222	17391	271.05338	-24.39583	18.923	16.202	2.59580	0.38	1.11	0.67	2.04	29.537	-	-	-
719	12850	271.16208	-24.45462	17.442	15.182	2.59596	0.56	0.97	1.09	2.20	29.922	-	W	N
609	11091	271.12683	-24.48144	18.289	15.930	2.65633	0.50	1.67	0.57	1.67	29.783	-	-	-
793	13601	271.19071	-24.44252	18.475	16.056	2.67708	0.47	1.77	0.51	1.60	30.693	-	-	-
174	29683	271.03875	-24.27527	18.206	16.082	2.70134	0.71	4.63	0.46	1.30	29.334	-	-	-
287	15179	271.06596	-24.41885	17.291	15.384	2.76327	0.98	3.57	0.85	1.60	30.297	N	-	N
737	19631	271.16600	-24.37405	18.550	15.896	2.78590	0.39	0.95	0.83	2.24	29.761	-	-	-

TABLE 4 — *Continued*

ID X-ray	ID WFI	RA [deg]	DEC [deg]	V [mag]	I [mag]	Period [d]	Mass [M_{\odot}]	Age [Myrs]	L_{bol} [L_{\odot}]	Radius [R_{\odot}]	$\log(L_X)$ [erg s^{-1}]	IR excess?	H α class? ^a	SB2?
277	20625	271.06504	-24.36438	17.480	15.620	2.80857	1.04	5.97	0.68	1.40	29.706	N	-	N
548	19806	271.11492	-24.37238	17.951	15.767	2.80874	0.63	2.26	0.64	1.60	29.827	-	-	-
627	16783	271.13079	-24.40135	18.489	16.182	2.83195	0.54	2.57	0.45	1.43	29.298	-	-	-
030	16985	270.97525	-24.39934	17.743	15.699	2.87938	0.79	3.55	0.62	1.47	30.663	N	-	N
391	13087	271.08750	-24.45083	17.310	14.726	2.87938	0.40	0.17	1.78	3.23	30.136	-	W	N
590	16802	271.12229	-24.40117	18.114	15.826	2.92877	0.55	1.77	0.62	1.67	29.553	-	-	-
741	16944	271.16775	-24.39960	16.389	14.427	3.08708	0.86	0.90	2.04	2.56	30.411	-	-	N
042	28541	270.98471	-24.28459	19.978	16.881	3.10201	0.33	2.34	0.26	1.32	29.477	-	-	-
654	13251	271.13983	-24.44821	17.390	15.236	3.14373	0.65	1.38	1.03	2.01	31.065	-	W	N
805	20587	271.19904	-24.36477	18.900	16.330	3.18901	0.40	1.78	0.41	1.55	29.511	-	-	-
451	11471	271.09730	-24.47562	17.726	15.938	3.23251	1.00	11.14	0.47	1.15	29.699	N	-	N
239	27870	271.05725	-24.29087	17.882	15.561	3.24160	0.52	1.24	0.79	1.93	30.060	-	-	N
128	19465	271.02250	-24.37583	20.690	17.309	3.26329	0.29	2.70	0.19	1.21	29.399	-	-	-
335	12639	271.07829	-24.45799	16.461	14.824	3.26329	1.39	3.97	1.49	1.84	29.923	Y	-	N
742	13457	271.16854	-24.44493	17.594	15.430	3.29487	0.65	1.65	0.87	1.85	30.795	N	-	N
102	19724	271.01130	-24.37319	18.489	16.242	3.32666	0.59	3.29	0.42	1.34	29.867	-	-	-
806	17811	271.19937	-24.39184	15.680	13.928	3.39273	1.25	0.95	3.35	2.93	30.534	N	-	Y
704	16450	271.15467	-24.40486	16.686	15.041	3.46127	1.30	5.27	1.14	1.64	30.268	-	-	-
848	13902	271.22192	-24.43753	20.967	17.433	3.48187	0.27	2.91	0.17	1.16	30.126	-	-	-
092	27121	271.00917	-24.29820	18.735	16.509	3.51774	0.61	5.14	0.33	1.16	29.792	-	-	-
375	18735	271.08500	-24.38305	17.747	15.044	3.64517	0.38	0.36	1.53	3.03	29.995	N	-	N
331	26667	271.07754	-24.30389	20.270	17.475	3.65988	0.36	5.58	0.15	0.93	29.349	-	-	-
378	25120	271.08517	-24.32323	17.059	14.998	3.69966	0.74	1.43	1.21	2.08	30.549	N	W	N
821	13288	271.20850	-24.44759	18.996	16.462	3.72463	0.42	2.19	0.36	1.42	30.113	-	-	-
149	23122	271.03238	-24.34145	18.188	15.455	3.74031	0.38	0.49	1.43	2.94	29.780	-	-	-
761	13043	271.17712	-24.45161	18.153	15.794	3.76556	0.50	1.44	0.65	1.78	29.922	-	-	-
733	12716	271.16467	-24.45663	18.052	15.795	3.80740	0.57	1.84	0.63	1.66	30.168	-	-	-
227	19208	271.05442	-24.37863	17.340	15.601	3.98425	1.10	8.15	0.65	1.32	29.845	N	-	N
424	19339	271.09205	-24.37709	18.707	16.287	3.98425	0.47	2.27	0.41	1.44	30.110	-	-	-
002	16351	270.94654	-24.40602	16.109	14.409	4.07912	1.33	1.92	2.16	2.30	30.116	Y	C	N
508	20209	271.10671	-24.36860	17.367	15.644	4.07912	1.10	9.04	0.62	1.29	30.135	-	-	-
729	13000	271.16438	-24.45250	17.641	15.223	4.07936	0.47	0.85	1.09	2.37	30.115	Y	-	N
722	14638	271.16229	-24.42590	17.791	15.770	4.12851	0.83	4.27	0.59	1.41	31.387	N	-	N
727	19423	271.16383	-24.37624	17.619	15.440	4.12851	0.63	1.56	0.87	1.87	30.031	N	-	N
496	16083	271.10492	-24.40906	19.150	16.314	4.17861	0.37	1.46	0.46	1.72	29.710	-	-	-
811	10889	271.20171	-24.48443	15.901	14.011	4.17886	0.99	0.73	3.03	2.99	30.711	N	-	Y
491	15630	271.10408	-24.41368	17.621	15.479	4.28333	0.67	1.94	0.81	1.77	29.477	-	-	-
396	31409	271.08788	-24.26252	18.601	16.332	4.30846	0.57	3.48	0.39	1.30	30.199	-	-	-
866	27189	271.23584	-24.29743	18.780	16.443	4.31516	0.52	3.27	0.36	1.29	29.900	-	-	-
441	17020	271.09513	-24.39901	16.731	14.908	4.33729	1.10	2.47	1.33	1.92	30.403	-	-	-
211	25505	271.05025	-24.31940	17.495	15.275	4.42037	0.59	1.13	1.00	2.07	30.270	N	-	N
208	13705	271.04971	-24.44113	16.556	14.358	4.56861	0.60	0.55	2.38	3.17	30.593	Y	C	N
364	31545	271.08371	-24.26165	17.799	15.583	4.59957	0.60	1.57	0.76	1.79	29.919	-	-	Y
190	35380	271.04259	-24.23360	18.227	15.949	4.72734	0.56	2.10	0.55	1.56	29.747	-	-	-
090	36784	271.00617	-24.22320	16.023	14.258	4.80593	1.21	1.32	2.46	2.53	30.675	N	-	N
124	12576	271.02025	-24.45901	17.852	15.973	4.89494	1.00	9.48	0.49	1.20	29.755	-	-	N
327	12091	271.07654	-24.46673	18.840	16.243	4.96588	0.40	1.53	0.47	1.66	30.010	-	-	-
864	22913	271.23463	-24.34341	18.563	16.156	5.01321	0.48	1.99	0.47	1.53	30.091	-	-	-
133	14903	271.02417	-24.42184	16.765	14.990	5.03891	1.19	3.25	1.25	1.82	30.012	Y	C	N
228	13933	271.05446	-24.43713	17.467	15.119	5.03891	0.50	0.81	1.21	2.42	30.394	Y	-	N
752	12351	271.17362	-24.46293	19.644	17.034	5.03921	0.39	3.85	0.21	1.10	29.888	-	-	-
763	16673	271.17946	-24.40247	18.526	16.311	5.03921	0.62	4.09	0.39	1.27	29.715	-	-	-
167	27078	271.03746	-24.29877	19.010	16.609	5.08013	0.48	3.40	0.31	1.24	29.219	-	-	-
065	19335	270.99617	-24.37721	18.448	16.229	5.19160	0.61	3.56	0.42	1.32	30.172	-	-	-
716	19552	271.15992	-24.37495	18.054	15.660	5.19191	0.48	1.23	0.73	1.91	30.345	-	-	-
764	15568	271.17963	-24.41438	17.586	15.794	5.19191	1.07	9.44	0.58	1.25	29.642	-	-	N
188	32594	271.04213	-24.25421	18.694	16.222	5.24956	0.45	1.94	0.44	1.52	29.944	-	-	-
819	14410	271.20579	-24.42947	20.251	16.988	5.27179	0.31	2.11	0.26	1.38	30.122	-	-	-
860	16003	271.23154	-24.41001	17.257	15.071	5.27179	0.61	1.00	1.22	2.24	30.460	Y	W	N
461	29528	271.09904	-24.27648	17.289	15.490	5.31826	1.11	6.03	0.76	1.45	30.086	-	W	N
196	26466	271.04433	-24.30633	18.864	16.645	5.40268	0.62	6.50	0.29	1.08	29.898	-	-	-
403	12374	271.08880	-24.46256	15.765	13.839	5.43882	0.93	0.57	3.52	3.29	30.850	N	-	Y
393	17986	271.08788	-24.39037	16.923	14.734	5.52655	0.61	0.74	1.66	2.62	30.548	Y	C	N
608	21076	271.12679	-24.36010	17.519	15.263	5.52687	0.56	1.06	1.01	2.11	29.980	-	-	-
270	25540	271.06329	-24.31863	16.762	15.180	5.57981	1.30	7.60	1.05	1.51	29.923	-	-	-
613	23385	271.12750	-24.33917	17.981	15.746	5.68163	0.58	1.82	0.66	1.68	30.345	-	-	-
123	13518	271.01980	-24.44375	17.203	15.382	5.80756	1.11	4.86	0.86	1.54	29.932	Y	W	N
775	33939	271.18388	-24.24413	16.197	14.594	5.87755	1.48	3.31	1.84	2.02	30.150	N	-	N
219	33415	271.05317	-24.24819	18.801	16.411	5.97138	0.49	2.75	0.37	1.35	29.467	-	-	-
008	16866	270.95550	-24.40045	20.295	16.917	6.01133	0.29	1.56	0.36	1.68	29.764	-	-	-
459	19278	271.09879	-24.37772	16.472	14.509	6.01169	0.86	0.98	1.89	2.47	30.666	N	-	N
607	14588	271.12671	-24.42664	19.743	17.167	6.01169	0.40	4.56	0.19	1.04	29.713	-	-	-
320	26045	271.07463	-24.31175	19.635	16.889	6.18852	0.38	3.13	0.23	1.19	29.554	-	-	-
464	28903	271.10009	-24.28160	18.447	16.002	6.18852	0.46	1.61	0.53	1.66	29.392	-	-	-
611	28535	271.12725	-24.28463	17.355	15.558	6.19815	1.10	6.68	0.71	1.40	29.975	-	-	N

TABLE 4 — *Continued*

ID X-ray	ID WFI	RA [deg]	DEC [deg]	V [mag]	I [mag]	Period [d]	Mass [M_{\odot}]	Age [Myrs]	L_{bol} [L_{\odot}]	Radius [R_{\odot}]	$\log(L_X)$ [erg s^{-1}]	IR excess?	H α class? ^a	SB2?
220	18366	271.05305	-24.38689	17.754	15.642	6.22993	0.70	2.69	0.68	1.60	29.881	-	-	-
414	14708	271.09067	-24.42486	17.484	15.507	6.22993	0.88	3.36	0.75	1.56	29.863	-	-	-
295	25906	271.06763	-24.31328	18.142	15.394	6.30312	0.38	0.44	1.44	2.96	29.715	N	-	Y
586	19263	271.12221	-24.37795	19.549	16.819	6.46540	0.38	2.90	0.25	1.23	29.197	-	-	-
734	18322	271.16462	-24.38729	20.969	17.633	6.46540	0.28	3.67	0.15	1.03	29.706	-	-	-
870	15444	271.24025	-24.41573	17.620	15.450	6.46540	0.64	1.64	0.85	1.84	29.441	Y	-	N
791	28774	271.18859	-24.28261	17.109	15.211	6.55573	0.98	2.87	1.00	1.73	30.052	-	W	N
093	30830	271.00925	-24.26704	19.580	17.088	6.56195	0.43	4.92	0.20	1.04	29.764	-	-	N
568	15914	271.11950	-24.41090	17.842	15.640	6.58973	0.61	1.77	0.72	1.73	29.411	-	-	N
604	23446	271.12505	-24.33867	17.080	15.019	6.68427	0.74	1.46	1.19	2.06	30.408	N	-	N
662	26358	271.14163	-24.30758	18.450	16.216	6.68427	0.59	3.30	0.43	1.35	30.110	-	-	-
070	28502	270.99934	-24.28496	20.087	17.309	6.82442	0.37	4.76	0.17	1.00	30.149	-	-	-
107	13412	271.01221	-24.44570	17.119	15.038	6.85292	0.72	1.46	1.17	2.07	30.405	N	W	N
790	17154	271.18850	-24.39773	19.244	16.801	6.85332	0.46	3.94	0.26	1.15	29.851	-	-	-
081	29462	271.00246	-24.27708	18.615	16.507	6.96370	0.75	9.35	0.30	1.04	29.898	-	-	-
744	00780	271.16942	-24.46403	16.565	14.628	6.99319	0.90	1.20	1.70	2.31	30.299	-	-	-
552	27280	271.11613	-24.29670	18.696	16.026	7.10204	0.39	1.04	0.73	2.11	29.140	-	-	-
779	31670	271.18434	-24.26057	17.588	15.561	7.10204	0.80	3.04	0.71	1.56	29.802	Y	C	N
114	24596	271.01709	-24.32810	18.441	16.066	7.24188	0.49	1.88	0.51	1.58	30.103	-	-	-
711	18265	271.15821	-24.38786	18.717	16.345	7.29077	0.50	2.62	0.39	1.38	29.851	-	-	-
460	27185	271.09892	-24.29754	17.242	15.124	7.39931	0.68	1.42	1.11	2.06	30.327	N	-	N
242	23073	271.05775	-24.34196	18.834	16.323	7.56374	0.43	1.99	0.41	1.49	30.025	-	-	-
258	23805	271.06129	-24.33539	19.562	16.970	7.56374	0.40	3.56	0.23	1.14	29.760	-	-	-
096	36232	271.01038	-24.22714	19.651	17.107	7.58269	0.40	4.34	0.20	1.06	29.583	-	-	-
170	23419	271.03808	-24.33886	17.094	14.977	7.73565	0.68	1.24	1.27	2.20	30.171	N	-	Y
148	20559	271.03217	-24.36509	19.539	16.936	7.78741	0.39	3.42	0.23	1.16	29.259	-	-	-
212	15682	271.05021	-24.41315	20.130	17.447	7.78741	0.38	6.00	0.15	0.92	29.932	-	-	-
298	16706	271.06884	-24.40202	18.023	15.936	7.78741	0.75	4.37	0.51	1.35	30.149	-	-	-
799	11957	271.19313	-24.46845	18.507	16.087	7.78787	0.47	1.83	0.49	1.58	29.683	-	-	-
856	13906	271.22883	-24.43747	20.593	17.255	7.78787	0.29	2.15	0.25	1.38	29.701	-	-	-
589	13072	271.12233	-24.45110	18.635	16.157	7.96898	0.45	1.79	0.47	1.57	30.083	-	-	-
641	20027	271.13500	-24.37040	18.652	16.207	7.96898	0.46	1.99	0.45	1.51	29.965	-	-	-
794	13161	271.19063	-24.44965	19.127	16.382	7.96898	0.38	1.44	0.48	1.73	29.421	-	-	-
800	13652	271.19483	-24.44175	19.228	16.300	7.96898	0.35	1.45	0.45	1.74	29.760	-	-	-
865	15997	271.23633	-24.41007	17.368	15.031	7.96898	0.51	0.77	1.30	2.49	29.669	N	-	N
362	22761	271.08350	-24.34487	19.922	16.859	8.10401	0.34	2.40	0.25	1.31	29.723	-	-	-
656	16726	271.14004	-24.40183	19.161	16.544	8.15872	0.39	2.13	0.34	1.42	29.650	-	-	-
236	27255	271.05600	-24.29698	19.580	16.935	8.30167	0.39	3.37	0.23	1.16	29.778	-	-	-
569	18719	271.11983	-24.38318	19.444	16.711	8.35771	0.38	2.56	0.28	1.29	29.720	-	-	-
703	16098	271.15433	-24.40885	17.573	15.431	8.35771	0.67	1.83	0.85	1.81	29.308	Y	-	N
801	12881	271.19754	-24.45418	18.455	16.111	8.35771	0.51	2.12	0.48	1.52	30.152	-	-	-
697	28698	271.15292	-24.28334	20.467	17.503	8.48620	0.34	4.70	0.15	0.97	29.421	-	-	-
112	22030	271.01550	-24.35152	17.768	15.824	8.50921	0.94	6.07	0.56	1.32	30.005	Y	-	N
797	26643	271.19176	-24.30418	19.439	16.901	8.52245	0.41	3.48	0.24	1.17	29.710	-	-	-
179	30020	271.04063	-24.27289	18.602	16.337	8.53053	0.57	3.55	0.39	1.29	29.961	-	-	-
171	17601	271.03813	-24.39376	19.740	17.030	8.56615	0.38	3.66	0.21	1.12	30.139	-	-	-
297	15923	271.06825	-24.41087	16.771	14.774	8.56615	0.81	1.19	1.48	2.23	30.433	-	C ^b	-
471	28967	271.10113	-24.28102	17.920	15.845	8.72740	0.76	3.98	0.55	1.40	29.909	-	-	N
078	15644	271.00084	-24.41358	19.846	17.106	8.78579	0.38	3.94	0.20	1.08	29.371	-	-	-
310	19592	271.07213	-24.37446	16.918	14.953	8.78579	0.86	1.64	1.26	2.02	29.870	Y	C	N
474	22856	271.10180	-24.34399	19.132	16.594	8.78579	0.42	2.50	0.32	1.34	30.059	-	-	-
482	15289	271.10267	-24.41755	18.844	16.218	8.78579	0.39	1.39	0.52	1.76	30.001	-	-	-
675	19178	271.14567	-24.37886	18.005	15.822	8.78631	0.63	2.43	0.61	1.57	29.880	-	-	-
694	19318	271.15100	-24.37736	18.459	16.250	8.78631	0.62	3.86	0.42	1.30	29.836	-	-	-
820	14135	271.20583	-24.43403	20.055	16.980	8.78631	0.33	2.60	0.23	1.26	29.805	-	-	-
316	28399	271.07392	-24.28597	17.385	15.323	8.95707	0.75	2.06	0.89	1.78	29.964	Y	-	N
774	24659	271.18355	-24.32762	16.297	14.391	8.97100	0.94	1.00	2.13	2.54	30.379	Y	C	N
186	16389	271.04209	-24.40553	19.786	16.988	8.97914	0.37	3.33	0.22	1.15	29.239	-	-	-
344	19620	271.08025	-24.37413	18.673	16.284	9.01700	0.49	2.37	0.41	1.43	29.384	-	-	-
215	23945	271.05121	-24.33419	18.310	16.109	9.19915	0.63	3.30	0.47	1.38	30.032	-	-	-
176	20164	271.03938	-24.36923	19.789	17.108	9.26070	0.38	4.04	0.20	1.08	29.986	-	-	-
319	16606	271.07459	-24.40308	19.615	16.410	9.26070	0.32	1.56	0.38	1.67	30.155	-	-	-
232	35944	271.05517	-24.22937	20.765	17.535	9.45468	0.30	3.57	0.15	1.06	29.580	-	-	-
376	28153	271.08500	-24.28808	18.310	15.682	9.45468	0.39	0.87	0.98	2.43	30.256	-	-	-
530	25566	271.11055	-24.31784	17.691	15.455	9.46939	0.58	1.31	0.86	1.92	30.126	Y	-	N
598	23906	271.12396	-24.33444	19.752	16.720	9.46939	0.34	2.22	0.28	1.36	29.406	-	-	-
353	11968	271.08180	-24.46846	19.212	16.748	9.51794	0.45	3.54	0.28	1.19	30.066	-	-	-
740	14524	271.16788	-24.42765	19.942	17.177	9.51851	0.37	4.12	0.19	1.06	29.425	-	-	-
027	21348	270.97446	-24.35771	18.123	16.013	9.72481	0.73	4.45	0.48	1.33	29.673	-	-	-
254	31912	271.06046	-24.25894	17.833	15.819	9.72481	0.84	4.72	0.56	1.37	30.076	-	-	N
266	13513	271.06184	-24.44386	18.666	16.247	9.78988	0.47	2.16	0.43	1.47	29.890	-	-	-
272	13522	271.06375	-24.44362	17.547	15.536	9.78988	0.83	3.11	0.73	1.57	30.347	N	-	N
674	18941	271.14554	-24.38109	17.963	15.728	9.79046	0.58	1.79	0.67	1.69	29.872	Y	-	N
101	27090	271.01142	-24.29856	18.965	16.788	10.01084	0.68	10.07	0.25	0.97	29.485	-	-	-
612	18481	271.12742	-24.38568	18.194	15.925	10.07842	0.56	2.08	0.57	1.57	30.659	-	-	-

TABLE 4 — *Continued*

ID X-ray	ID WFI	RA [deg]	DEC [deg]	V [mag]	I [mag]	Period [d]	Mass [M_{\odot}]	Age [Myrs]	L_{bol} [L_{\odot}]	Radius [R_{\odot}]	$\log(L_X)$ [erg s^{-1}]	IR excess?	H α class? ^a	SB2?
676	17674	271.14671	-24.39308	17.718	15.613	10.07842	0.71	2.65	0.69	1.61	30.056	-	-	-
413	25554	271.09084	-24.31812	18.633	16.096	10.33024	0.42	1.53	0.50	1.68	29.091	-	-	-
762	25591	271.17905	-24.31719	18.848	16.386	10.33024	0.46	2.34	0.38	1.41	30.248	-	-	-
127	17541	271.02192	-24.39420	17.808	15.768	10.70768	0.80	3.97	0.59	1.42	30.043	Y	-	N
645	30029	271.13700	-24.27280	18.925	16.688	10.99671	0.60	6.25	0.28	1.08	29.684	-	-	-
652	16587	271.13917	-24.40321	19.036	16.755	11.05375	0.57	5.86	0.27	1.07	29.749	-	-	-
871	18807	271.24154	-24.38240	19.621	16.540	11.42221	0.33	1.89	0.32	1.48	29.994	-	-	-
484	23229	271.10280	-24.34063	16.554	14.668	11.75510	0.98	1.48	1.65	2.21	30.481	-	-	-
300	19113	271.06900	-24.37950	20.943	17.837	11.81538	0.30	5.31	0.11	0.89	29.766	-	-	-
125	29284	271.02117	-24.27838	16.276	14.539	12.18647	1.27	2.05	1.91	2.19	30.043	Y	-	N
521	19014	271.10834	-24.38033	17.954	15.801	12.59194	0.67	2.73	0.61	1.54	30.118	-	-	-
117	25523	271.01783	-24.31899	17.651	15.532	13.09110	0.69	2.29	0.76	1.69	29.718	-	-	-
863	26449	271.23421	-24.30651	20.023	17.310	14.82165	0.38	4.98	0.17	0.98	29.544	-	-	-
341	20091	271.07963	-24.36985	18.027	15.837	16.31647	0.63	2.40	0.60	1.56	29.676	-	-	-
835	16451	271.21467	-24.40484	19.042	15.961	16.31744	0.33	0.48	1.08	2.70	30.138	-	-	-
622	30332	271.12930	-24.27067	20.204	16.888	17.94200	0.30	1.83	0.30	1.50	30.329	-	-	-
303	21086	271.06938	-24.36001	16.124	14.246	18.03399	1.00	0.95	2.44	2.67	30.451	Y	C	N
392	22580	271.08796	-24.34644	16.780	14.786	18.03399	0.81	1.22	1.46	2.21	30.271	-	-	-
714	18221	271.15963	-24.38824	21.826	18.047	18.03506	0.23	3.88	0.11	0.96	29.500	-	-	-
503	13456	271.10538	-24.44494	18.802	16.188	18.95596	0.40	1.40	0.51	1.75	29.873	-	-	-
875	15993	271.24425	-24.41012	17.521	15.020	19.03701	0.43	0.68	1.43	2.81	29.793	-	-	-

^a C denotes Classical T-Tauri stars while W identifies Weak-lined T-Tauri stars.^b These H α classifications are taken from Arias et al. (2007); all others come from Prisinzano et al. (2007).

TABLE 5
PARAMETERS OF THE 46 CLUSTER MEMBERS WITH POSSIBLE ROTATION PERIODS

ID X-ray	ID WFI	RA [deg]	DEC [deg]	V [mag]	I [mag]	Period [d]	Mass [M_{\odot}]	Age [Myrs]	L_{bol} [L_{\odot}]	Radius [R_{\odot}]	$\log(L_X)$ [erg s^{-1}]	IR excess?	H α class? ^a	SB2?
217	25571	271.05200	-24.31766	17.959	15.489	0.3999630	0.45	1.01	0.84	2.12	29.890	-	-	-
425	21654	271.09217	-24.35480	17.818	15.830	0.6353953	0.88	5.26	0.56	1.34	29.822	-	-	-
581	13973	271.12150	-24.43629	19.875	16.704	0.6393026	0.32	1.95	0.30	1.45	29.406	-	-	-
126	15028	271.02154	-24.42041	19.131	16.418	0.6978532	0.38	1.57	0.44	1.64	29.490	-	-	-
732	28075	271.16463	-24.28881	17.645	15.552	0.7891157	0.73	2.56	0.73	1.64	29.601	Y	W	N
307	30975	271.07117	-24.26600	19.945	17.015	0.8065604	0.35	3.05	0.22	1.18	29.465	-	-	-
371	19029	271.08471	-24.38020	18.592	15.934	0.8771817	0.39	0.98	0.80	2.21	30.245	-	-	-
758	21152	271.17558	-24.35950	18.223	15.931	0.9286347	0.55	1.99	0.56	1.59	29.923	-	-	-
184	24932	271.04159	-24.32497	16.800	14.748	0.9780704	0.74	1.13	1.51	2.32	29.363	Y	-	Y
261	21719	271.06155	-24.35429	18.918	16.246	0.9931765	0.39	1.30	0.55	1.84	29.171	-	-	-
248	21246	271.05884	-24.35849	18.381	15.887	0.9960637	0.44	1.36	0.59	1.80	29.379	-	-	-
012	19726	270.95917	-24.37323	15.863	14.173	1.0167534	1.36	1.48	2.69	2.55	29.807	Y	C	N
606	18471	271.12633	-24.38579	18.606	16.052	1.2151284	0.41	1.43	0.52	1.73	29.377	-	-	-
579	20605	271.12142	-24.36462	14.943	13.479	1.4963590	2.09	1.95	4.96	2.96	30.891	N	-	Y
500	23609	271.10534	-24.33733	17.214	15.058	1.9369204	0.64	1.13	1.22	2.19	30.066	N	-	N
343	21103	271.08025	-24.35984	16.331	14.507	2.4474707	1.10	1.49	1.93	2.31	30.027	N	-	N
824	13903	271.21058	-24.43753	18.306	15.760	2.4652245	0.41	1.15	0.68	1.97	29.941	-	-	-
440	19698	271.09509	-24.37335	20.006	16.907	3.0869000	0.33	2.42	0.25	1.30	29.528	-	-	-
377	18217	271.08505	-24.38833	19.888	17.253	3.3266592	0.39	4.94	0.17	1.00	29.369	-	-	-
678	28104	271.14721	-24.28850	18.813	16.478	3.3752277	0.52	3.46	0.34	1.26	29.835	-	-	-
072	25460	271.00025	-24.31999	15.351	13.961	3.4380660	1.84	4.45	3.46	2.28	30.583	-	-	-
836	14959	271.21500	-24.42105	17.002	14.726	3.6845828	0.55	0.68	1.66	2.73	30.218	Y	C	N
069	38914	270.99759	-24.20661	15.708	14.146	3.8775140	1.66	2.31	2.82	2.41	30.488	-	-	Y
591	18597	271.12271	-24.38450	15.899	13.940	4.6940575	0.87	0.58	3.19	3.20	30.718	N	C	Y
599	14962	271.12429	-24.42103	19.808	17.245	4.7592528	0.40	5.05	0.17	1.00	29.855	-	-	-
032	23886	270.97529	-24.33478	20.309	17.412	5.4162100	0.35	4.66	0.16	0.99	29.740	-	-	-
363	19052	271.08350	-24.38004	16.143	14.354	5.5265468	1.17	1.40	2.24	2.44	30.442	-	W ^b	-
647	12995	271.13779	-24.45254	18.454	16.175	7.1388792	0.56	2.76	0.45	1.41	29.662	-	-	-
544	24884	271.11388	-24.32548	18.689	16.134	7.4108261	0.41	1.53	0.48	1.67	29.812	-	-	-
468	13134	271.10038	-24.45008	19.577	16.841	8.7857923	0.38	2.95	0.25	1.22	29.349	-	-	-
214	19826	271.05059	-24.37219	16.899	15.020	9.0169974	1.01	2.39	1.20	1.88	30.056	-	-	-
789	22239	271.18846	-24.34960	16.185	14.352	9.2134595	1.08	1.21	2.23	2.49	29.312	Y	-	N
058	13674	270.99367	-24.44153	19.185	16.016	9.2607000	0.32	0.88	0.79	2.39	30.276	-	-	-
264	27558	271.06183	-24.29384	18.243	15.937	10.0108380	0.54	1.93	0.56	1.60	29.886	-	-	-
731	13384	271.16442	-24.44602	18.757	15.917	10.7083188	0.37	0.61	1.24	2.79	29.979	-	-	-
555	12099	271.11650	-24.46659	18.978	15.841	11.4222067	0.33	0.34	1.07	2.71	29.539	-	-	-
578	22849	271.12130	-24.34411	16.941	14.804	11.7551035	0.66	0.97	1.55	2.44	30.450	N	-	N
433	25848	271.09409	-24.31404	18.744	16.164	12.6258519	0.40	1.50	0.48	1.68	29.757	-	-	-
553	00646	271.11633	-24.36901	16.739	14.947	12.6913407	1.16	2.90	1.29	1.86	29.782	-	-	-
218	19026	271.05284	-24.38029	20.409	17.198	13.7058360	0.31	2.62	0.21	1.24	29.264	-	-	-
840	14749	271.21825	-24.42408	19.551	16.488	13.7066480	0.34	1.82	0.33	1.51	31.284	-	-	-
347	14041	271.08084	-24.43536	17.852	15.767	14.8976478	0.75	3.46	0.59	1.47	30.149	Y	-	N
597	21779	271.12358	-24.35379	17.618	15.390	15.5757364	0.59	1.25	0.91	1.97	29.915	-	-	-
073	21526	271.00050	-24.35593	18.079	15.685	17.9141320	0.48	1.26	0.71	1.88	29.797	-	-	Y
571	22057	271.12009	-24.35124	19.021	16.512	17.9420000	0.43	2.43	0.34	1.37	29.941	-	-	-
562	14558	271.11771	-24.42712	17.922	15.618	19.0370111	0.54	1.36	0.75	1.85	29.806	-	-	N

^a C denotes Classical T-Tauri stars while W identifies Weak-lined T-Tauri stars.

^b These H α classifications are taken from Arias et al. (2007); all others come from Prisinzano et al. (2007).

TABLE 6
STATISTICAL COMPARISONS OF ROTATION PERIODS

	N	$\langle P \rangle$	KS prob.	t prob.
NIR excess	27	6.253		
No NIR excess	39	3.679	0.0125	0.00160
CTT	10	7.316		
WTT	15	3.376	0.0248	0.00590
Low-mass	98	6.357		
High-mass	146	4.929	0.00104	0.00511
Young	92	4.890		
Old	152	5.873	0.0136	0.0575
Northwest	79	5.199		
Southeast	70	6.238	0.0115	0.117
Northeast	30	5.982		
Southwest	65	4.858	0.141	0.175

TABLE 7
STATISTICAL COMPARISONS OF X-RAY LUMINOSITIES

	N	$\langle \log(L_X/L_{\text{bol}}) \rangle$	KS prob.	t prob.
Fast	79	-3.556		
Slow	165	-3.372	0.000267	0.000338
P_{rot}	244	-3.432		
No P_{rot}	458	-3.632	0.000620	6.28×10^{-6}

TABLE 8
SLOPES OF THE PERIOD–MASS RELATIONSHIP FOR YOUNG CLUSTERS

Cluster	Age [Myr]	slope
N6530	1.65	-0.55 ± 0.39
ONC	2	0.48 ± 0.35
N2264	3	1.24 ± 0.30
N2362	3.5	1.55 ± 0.28
IC348	4.5	2.52 ± 0.21
N2547	40	2.86 ± 0.38
N2516	150	3.15 ± 0.23

NOTE. — Slopes are from linear fits to the upper envelope of rotation periods versus mass, of the form $\log P = a \times M + b$, where P is in days and M is in M_{\odot} . Ages are from Mayne et al. (2007) and Mayne & Naylor (2008), except for NGC 6530 whose age here is determined from the linear relationship fitted to the other clusters. See §5.